Gravity-Driven Differences in Fluvial Sediment Transport on Mars and Earth

Lisanne Braat [1,2], Muriel Z. M. Brückner [3], Elliot Sefton-Nash [1], Michael P. Lamb [2]

[1]European Space Agency (ESA), Noordwijk, The Netherlands
[2]California Institute of Technology (Caltech), Pasadena CA, United States of America
[3]University of Exeter, Exeter, United Kingdom

Key Points:

- Fluvial sediment transport rates are higher on Mars than on Earth for the same discharge and channel geometry.
- Gravity affects suspended sediment transport more than bed load transport and could hence lead to differences in morphology and stratigraphy.
- Total load sediment transport equations should be avoided on other planets and moons due to simplified attribution of gravity.

Corresponding author: Lisanne Braat, `lisannebraat@gmail.com`

Abstract

There is abundant evidence from fluvial landforms and deposits that Mars had rivers that actively transported sediment and shaped its surface. Sediment transport equations are playing a key role in quantifying river processes from these observations, which continue to increase in quality and quantity. In this study, we review sediment transport equations developed on Earth and isolate the effect of gravity for the case of an alluvial channel. We compare 33 formulas used to calculate the sediment transport rate, under transport-limited conditions, for grain sizes that range from silt to boulders and a lognormal sediment distribution. Results indicate that for a given discharge, channel morphology and grain size, the lower gravity on Mars compared to Earth results in: 1) larger grains mobilised on Mars and transported in suspension, and 2) larger suspended sediment transport rates on Mars and therefore larger total transport rates. Importantly, the effect of gravity is different for bed load and suspended load, with nonlinearity at the bed load-suspended load transition zone. Therefore, typical total-load transport relations that do not distinguish between bedload and suspended load are not appropriate for other planets as they simplify the effect of gravity. Gravity-driven differences in fluvial sediment transport should produce differences in sediment sorting, morphology and stratigraphy between Earth and Mars. Additionally, our results show how Earth-derived fluvial sediment transport theory can be applied beyond Mars to other planets and moons.

Plain Language Summary

There is much evidence that Mars had rivers that actively transported sediment and shaped its surface. Preserved ancient landscapes altered by water provide valuable insights into past processes on the planet's surface and the presence of water. To better understand these landforms, we rely on knowledge gained from systems on Earth. However, is it fair to do so when the gravity on Mars is much lower? How does gravity affect sediment transport and the landforms created by water? In this study, we isolate the effect of gravity on sediment transport by water with an analytical river model. We used 32 sediment transport formulas to compare sediment transport rates on Earth and Mars for the same conditions except gravity. The results show that larger grains are picked up by the flow on Mars and the transport rate of sediment travelling in suspension is higher, and therefore total transport as well. Because grains transported near and on the bed are less affected than the grains in suspension, the effect of gravity varies with the way of transport and hence grain size. Therefore, gravity-driven differences in sediment transport by water should produce differences in sediment sorting, morphology and stratigraphy between Earth and Mars.

Keywords

Mars, fluvial geomorphology, sediment transport, suspended load, bedload, gravity

1 Introduction

Similar to Earth, surface dynamics have shaped the landscape of Mars. Since the first Viking images in 1976, many landforms at the surface of Mars have been identified that indicate ancient fluvial activity (Carr, 2012), such as depositional river channels (Fig. 1A-C; e.g., Dickson et al., 2021), deltas (Fig. 1C-G; e.g., Malin & Edgett, 2003; Di Achille & Hynek, 2010; DiBiase et al., 2013; Hauber et al., 2013; S. A. Wilson et al., 2021; De Toffoli et al., 2021), alluvial fans (Fig. 1H; e.g., Moore & Howard, 2005; Kraal et al., 2008; S. A. Wilson et al., 2021), valleys and valley networks (Fig. 1I; e.g., Hynek & Phillips, 2003; Hynek et al., 2010; Bahia et al., 2022), open (or chain) crater lakes (Fig. 1J; e.g., Cabrol & Grin, 1999, 2001, 2003; Fassett & Head III, 2008) and outflow channels (Fig. 1K-L; e.g., Sharp, 1973; Baker & Milton, 1974; Harrison & Grimm, 2008). Further evidence comes from the Curiosity, Opportunity and Perseverance rovers. For example, by studying sedimentary strata in outcrops the Perseverance rover found evidence that the fan in Jezero crater could be of deltaic origin (Mangold et al., 2021) and Curiosity found evidence for an ancient lake in Gale crater (Grotzinger et al., 2015). These landforms formed as a result of entrainment, transport and deposition of sediments by a fluid, most likely liquid water (Murchie et al., 2009; Ehlmann et al., 2011). Thus, fluvial landforms and deposits potentially record habitable environments.

A key method to invert flow rates and timescales of these ancient rivers on Mars comes from sediment transport theory (Komar, 1979; Kleinhans, 2005; Grotzinger et al., 2013; Hayden et al., 2019). Sediment transport rates of ancient systems on Mars, however, are difficult to estimate since transport rates (the volume or mass of sediment moved over time through a river cross section) depend on grain size, transport mode, hydraulic conditions and gravity. Because the ancient fluvial systems on Mars are no longer active (e.g., Carr, 2012), all parameters to calculate sediment transport need to be estimated from deposits or landform morphology, similar to ancient inactive channels on Earth (Larsen & Lamb, 2016). This is not straight forward, as alteration has likely occurred by erosion, weathering and aeolian filling (Golombek et al., 2014). Mars provides extra challenges as these conditions must be determined from orbit or by rovers, therefore data type and availability are more limited resulting in fewer available methodologies for paleoenvironmental reconstruction. Nonetheless, if input parameters can be determined, we can systematically investigate sediment transport by applying physical and empirical transport equations derived for Earth under martian conditions.

Fluvial sediment transport on Earth has been studied since the early 20^{th} century and is typically divided into three modes (Einstein et al., 1940): Bed load, suspended load, and wash load. Bed load is the portion of the grains that is transported close to the bed by rolling, sliding and saltation. Smaller grains have transport trajectories influenced by turbulence and can be transported higher in the water column as suspended sediment. Wash load are the smallest grain sizes that are sufficiently fine that they are transported uniformly through the water column as a result of extremely low settling velocities. These transport modes are expected to occur on Mars, but with possible differences due to differences in gravitational acceleration (Komar, 1980; Burr et al., 2006), fluid density and viscosity (e.g., for the case of brines Lamb et al., 2012), and sediment densities (The surface of Mars is predominantly basaltic which has a higher density than quartz- and feldspar-dominated rocks that dominate Earth; e.g., Christensen et al., 2000). As sediment transport depends on gravitational acceleration, applying semi-empirical theory to Mars requires special consideration (Komar, 1979; Grotzinger et al., 2013). Gravity affects the sediment transport rate because it affects river hydraulics, which drives sediment transport, as well as sediment properties directly such as particle weight. For instance, on the one hand, the shear stress acting on the riverbed induces movement, and for a given river water depth and channel-bed slope, lower gravity should produce a lower bed shear stress. On the other hand, reduced weight of the sediment can counteract this trend, leading to reduced settling velocities and higher mobility.

Previous work has mostly focussed on the boundaries between transport modes: the initiation of sediment motion and the onset of significant suspension (Komar, 1980; Burr et al., 2006; Grotzinger et al., 2013; Amy & Dorrell, 2021). They found that bigger grains are more easily entrained on Mars compared to Earth (Komar, 1980; Grotzinger et al., 2013), that fluvial suspended sediment transport is more efficient on Mars (Amy & Dorrell, 2021) and that hyper-concentrated flows might be common (Komar, 1980; Burr et al., 2006). However, there has yet to be a systematic study on the effect of gravity on sediment transport rates within each transport mode. Transport rate equations are needed to estimate landform formation timescales (Komar, 1979; Kleinhans et al., 2010; Salese et al., 2020; Hayden et al., 2021), understand downstream sorting trends, and predict morphodynamic evolution of the martian surface. For Earth, several semi-empirical fluvial sediment transport relations (based on laboratory experiments or field data) have been developed to predict transport rates, depending on the near-bed sediment concentrations, shear stress induced by the flow and the sediment properties. Some of them have different functional forms and some have different dependencies on gravity (e.g., de Leeuw et al., 2020). In this study we analysed 20 different bed load transport equations, 11 suspended sediment entrainment equations, and 2 total load relations to better understand the effect of gravity on sediment transport rates between Earth and Mars. In particular we aim to: 1) test the response of hydraulic and associated sediment transport parameters for a range of values for gravitational acceleration; 2) estimate bed, suspended and total load sediment transport for a range of sediment grain sizes and a mixed grain size distribution; 3) compare the suitability of sediment transport relations for application to Mars.

2 Methods

In this section we first discuss our choice of model input parameters (section 2.1). Second, we use those input parameters to calculate the hydraulics, using equation 1–7 (section 2.2). Third, we use the hydraulic parameters to calculate several parameters related to sediment mobility using equation 8–13 (section 2.3). Using hydraulics and mobility parameters sediment transport is calculated. We show 30 transport relations in Table 2 that we use to evaluate bed load and suspended transport (section 2.4). Total load is calculated in two different ways. First, an empirical total load equation that implicitly combines bed and suspended load is used. Second, we explicitly combined a bed load and suspended sediment entrainment relations to calculate the total load (section 2.5). Lastly, we investigate the total transport rate of a sediment mixture (section 2.5).

2.1 Model input

We isolate the effects of gravity on fluvial sediment transport relations using analytical theory and a code in MATLAB R2022b. We assume an alluvial, single-thread, open channel with a fixed channel width and slope (Table 1). Although case studies could be done from orbital or rover data, we chose an idealised scenario so that the effect of gravity between Earth and Mars could be isolated with the exact same boundary conditions for fair comparison. In addition, we choose an arbitrary temperature to calculate viscosity and water density (Table 1). To calculate water flow, one more boundary condition is required. The most obvious parameter would either be water discharge or water depth. Keeping one or the other equal between model scenarios will lead to different outcomes. Though both were investigated in terms of hydraulics, we use discharge as a boundary condition (i.e., independent variable) to calculate sediment transport and the results for a water level boundary on transport are shown in the Appendix. For gravity, we use a value of 3.7 m/s^2 for Mars and 9.8 m/s^2 for Earth.

For sediment boundary conditions we use a sediment density of 2900 kg/m^3, which is in the density range of basalt (as in Burr et al., 2006; Amy & Dorrell, 2021). This igneous rock type is more common on Mars than on the continental areas on Earth, for which quartz 2650 kg/m^3 is more typical. The grain size range used varies from silt to large boulders. All input and boundary conditions that were used fall in a realistic range of conditions for Earth and Mars.

2.2 Hydraulic calculations

For an assumed discharge, Q, in m^3/s and channel width, W, in m we use mass balance to calculate water depth, h, in m assuming incompressible flow:

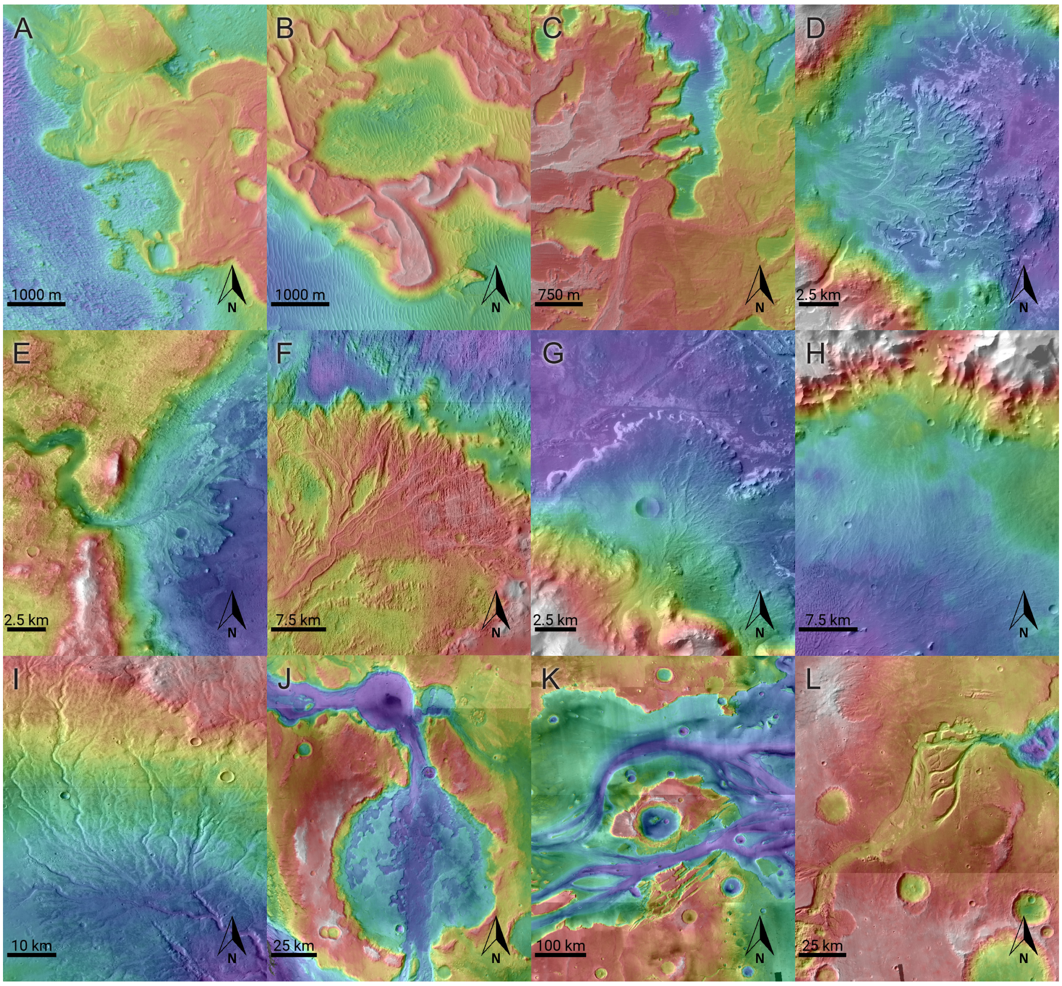

Figure 1. Examples of fluvial landforms on Mars. Inverted meandering depositional channel at (A-B) Aeolis Dorsa (HiRISE, 5.8°S, 205.4°W and 5.0°S, 205.1°W) and (C) Eberswalde (HiRISE, 23.8°S, 33.6°W). Deltas at (D) Eberswalde (MOLA/HRSC+CTX, 23.8°S, 33.6°W), (E) Jezero crater (CTX, 18.5°N, 282.7°W), (F) Aeolis Dorsa (MOLA/HRSC+CTX, 6.2°S, 208.6°W) and (G) Holden crater (MOLA/HRSC+CTX, 26.9°S, 34.5°W). (H) Alluvial fans (MOLA/HRSC+CTX, 21.4°S, 39.4°W), (I) valley drainage network (MOLA/HRSC+CTX, 42.1°S, 92.8°W), (J) chain lake system (MOLA/HRSC+CTX, 3.0°N, 16.1°W), (K) mega-outburst channels (MOLA/HRSC+CTX, 27°N, 58°W) and (L) outburst channel (MOLA/HRSC+CTX, 15.5°S, 38.6°W).

Table 1. Model boundary conditions

	Symbol	Value default scenario	Unit	Comment other scenarios
Boundary conditions flow				
Channel width	W	200	m	
Channel slope	S	0.001	m/m	
Water density	ρ	1000	kg/m^3	
Temperature	T	4	$^\circ C$	
Gravity acceleration	g	3.7, 9.8	m/s^2	Fig. 3 and 4 use a range: 1–12
Discharge	Q	2000	m^3/s	Fig. 3 and 7a use a range: 250–15000, Q is *calculated* in Fig. 4
Water depth	h	*calculated*	m	Fig. 4 and 8b use a range: 0.5–15
Velocity	u	*calculated*	m/s	Fig. 8c uses a range: 0.5–6.5
Shear stress	τ	*calculated*	m^2/s	Fig. 8d uses a range: 1–100
Boundary conditions sediment				
Sediment density	ρ_s	2900	kg/m^3	
Median grain size	D_{50}	63e-6–1e0	m	
Angle of repose	ϕ	30	$^\circ$	
Calculated parameters				
Relative density	R	1.9	–	
Kinematic viscosity	ν	1.54e-6	m^2/s	

$$h = \frac{Q}{Wu} \tag{1}$$

where u is the cross-sectionally and depth-averaged flow velocity in m/s. To find u we use the Darcy-Weisbach equation, which is a hydraulic resistance equation given by

$$u = u_* \sqrt{\frac{8}{f}} \tag{2}$$

where u_* is the bed shear velocity in m/s and f is a semi-empirical, non-dimensional friction factor that can be determined using the White-Colebrook function, which is a drag law and assumes hydraulic rough flow, written as

$$\sqrt{\frac{8}{f}} = 5.75 \log\left(\frac{12h}{k_s}\right) \tag{3}$$

where k_s is the Nikuradse bed roughness scale in m, here estimated to be 2.5 times the median grain diameter, D_{50}. Here we neglect larger bedforms and channel forms that can substantially increase flow resistance. Thus, the flow velocities we calculate should be seen as upper bounds. Conservation of momentum, under the assumption of steady and uniform flow, and a balance between the driving stress and the resisting stresses on the channel walls and bed yields

$$\tau = \rho g R_w S = \rho u_*^2 \tag{4}$$

where τ is the driving stress in N/m^2, ρ is the water density in kg/m^3, g is gravity in m/s^2, S is the channel bed slope in m/m and R_w is the hydraulic radius in m. The hydraulic radius for a rectangular channel with equivalent wall and bed roughness is given by

$$R_w = \frac{hW}{2h + W} \tag{5}$$

In addition to the hydraulic parameters, we calculated the Froude and the Reynolds number to investigate the effects of gravity on the transition between subcritical and supercritical, and laminar and turbulent flow, respectively:

$$Fr = \frac{u}{\sqrt{gh}} \tag{6}$$

$$Re = \frac{uh}{\nu} \tag{7}$$

where ν is the kinematic viscosity in m^2/s. This version of the Froude formula assumes open channel flow and a rectangular cross section.

2.3 Supporting fluvial sediment transport parameters

The mobility of the bed sediment can be expressed by the particle mobility parameter, i.e., Shields number, defined as

$$\theta = \frac{\tau}{(\rho_s - \rho)gD} \tag{8}$$

where ρ_s is the sediment density in kg/m^3 and D is the grain size in m. The Shields number, θ, is a nondimensionalisation of the bed shear stress. The initiation of motion of particles on the bed is commonly described by the Shields curve, which provides a critical Shields number, θ_{cr}, for the initiation of motion of each grain size. Over the years, many critical Shields curves have been formulated, of which we compared 18 in Appendix Section A1 (Mantz, 1977; Brownlie, 1981; Collins & Rigler, 1982; Komar & Clemens, 1986; Soulsby, 1997; Paphitis, 2001; Zanke, 2003; Cao et al., 2006; van Rijn, 2007; Beheshti & Ataie-Ashtiani, 2008; Simões, 2014; Kleinhans et al., 2017; Lapôtre & Ielpi, 2020). The comparison shows that most of the relations produce similar results (Fig. A1). Thus, in the subsequent calculations for sediment transport rates we used the physics-based relation of Zanke (2003) (Equation A1-A9). Although some sediment transport relations were designed to be used with a specific critical Shields number relation (Table 2), we use Zanke (2003) for all cases for purposes of comparison.

Bagnold (1966) defines the transition between bed load and suspension by the ratio of the downward component (settling velocity) and the upward component (turbulence) called the movability number k, where

$$k = \frac{w_s}{u_*} \tag{9}$$

and w_s is the settling velocity in m/s. Various values for k have been used in the past ([1–1.79] see Komar, 1980), however we use $k = 1$ for the suspension threshold for simplicity.

The velocity with which particles settle from the water column results from balancing the drag with the gravitational forces. We use the equation from Ferguson and Church (2004) given by

$$w_s = \frac{RgD^2}{C_1\nu + \sqrt{0.75C_2RgD^3}} \tag{10}$$

where R is the relative density, $(\rho_s{-}\rho)/\rho$, and C_1 and C_2 are constants. C_1 is the constant in Stokes' equation for laminar settling and C_2 is the constant asymptotic value of the drag coefficient. Both coefficients are related to the smoothness/roughness, angularity, and sphericity of the particles and we use 20 and 1, respectively (Ferguson & Church, 2004).

Additional parameters that were calculated are the particles Reynolds number Re_p, the Bonnefile parameter D_*, i.e., non-dimensional grain size, and the advection length L_A (Lamb et al., 2010) (Eq. 11–13). The particle Reynolds number and Bonnefile parameter are used in several sediment transport equations (Table 2). The advection length provides the average horizontal distance travelled by a particle before settling, which is important for morphology. Re_p, D_* and L_A are given by

$$Re_p = \frac{D^{3/2}\sqrt{Rg}}{\nu} \tag{11}$$

$$D_* = D\left(\frac{Rg}{\nu^2}\right)^{1/3} \tag{12}$$

$$L_A = \frac{uh}{w_s} \tag{13}$$

2.4 Bed and suspended load sediment transport equations

The hydraulic conditions and parameters related to sediment mobility, discussed above, serve as input for the sediment transport formulations. We used 20 bed load transport equations and 11 suspended sediment entrainment equations(Table 2). For all sediment transport calculations, we assume that transport is limited by the flow and sediment availability is unlimited. We evaluated these formulas using a single characteristic particle size for each scenario. Although riverbeds tend to have a mixture of particle sizes, it has been shown that finer particles tend to be sheltered between larger particles and thus are more difficult to move than expected (e.g., Parker, 1990). In addition, larger particles are more exposed to the flow, and can roll more easily over smaller particles, rendering their mobility greater than expected. The result of these grain hiding and exposure effects is that sediment transport of the entire mixture is often well characterized by using the median particle size, D_{50}, in the transport relation. The shields number in the bed load transport and entrainment relations should be the component due to skin friction, not due to form drag from bedforms or channel forms (e.g., Smith & McLean, 1977). Here we neglect bedforms and assume form drag is negligible for purposes of comparison. This assumption likely renders the sediment loads we calculate too large.

The volumetric bed load transport per unit channel width is defined in non-dimensional form (Table 2) using the Einstein parameter

$$\phi_b = \frac{q_b}{\sqrt{Rg}D^{3/2}} \tag{14}$$

where q_b in the bed load transport in m^2/s (m^3/s per m channel width). The suspended concentration profile, C, in m^3/m^3 depends on a near-bed reference concentration, C_a, in m^3/m^3 (Table 2) at the reference height above the bed, a, in m with which a Rouse profile is calculated. Here we assume an equilibrium suspension such that the near bed reference concentration is equal to the entertainment parameter, E_s. By integration and multiplication with the velocity profile, U, in m/s we obtain suspended transport:

$$q_s = \int_a^h C \cdot U dz = \int_a^h C_a \left(\frac{h-z}{z}\frac{a}{h-a}\right)^P \cdot \frac{u_*}{\kappa}\ln\left(\frac{z}{z_0}\right) dz \tag{15}$$

where z_0 is the zero-velocity level defined by $0.033{\cdot}k_s$ and P is the Rouse number (Rouse, 1937),

$$P = \frac{w_s}{\beta \kappa u_*} \tag{16}$$

where κ is the von Karman's constant taken to be 0.41 and the constant β taken to be 1 as it is likely near unity but can vary due to differences in turbulent diffusivity of the suspended sediment relative to momentum (e.g., de Leeuw et al., 2020). Since β and E_s are often calibrated together, it is best to use specific paired relations as given by the original studies. However, for purposes of comparison, here we assume β is unity for all cases.

2.5 Total sediment transport and mixtures

The total transport load is evaluated in two ways (Table 3). First, an empirical total load equation is used that implicitly combines bed and suspended load (Engelund & Hansen, 1967). Second, we follow de Leeuw et al. (2020), which is the most recent study to the authors knowledge that explicitly combines bed and suspended load transport to determine total transport.

The non-dimensional total transport rate, ϕ_t, by Engelund and Hansen (1967) is given by

$$\phi_t = \frac{0.1}{f}\theta^{2.5} \tag{17}$$

which can be converted to dimensional total transport, q_t, in m^2/s using Equation 14. To obtain total sediment transport in m^3/s the value is multiplied with the channel width.

The total transport by de Leeuw et al. (2020) is determined by explicitly adding the bed load transport rate, q_b, and the suspended transport rate, q_s. Following de Leeuw et al. (2020), bed load transport is determined using the relation by Fernandez Luque and van Beek (1976) (Table 2). The near-bed volumetric concentration within the bed load layer can then be calculated as

$$C_b = \frac{q_b}{h_b u_b} \tag{18}$$

where h_b is the bed load-layer thickness in m and u_b the bed load velocity in m/s described by

$$h_b = 0.6\left(Fr\left(\frac{D}{h}\right)^2\right)^{0.3} \tag{19}$$

$$u_b = 0.6u \tag{20}$$

determined from Chatanantavet et al. (2013) as in de Leeuw et al. (2020). Suspended transport is calculated by substituting C_b at elevation h_b for C_a and a in equation 15 (Table 3). For the calculation of total transport, we also substitute the Rouse number where $\beta = 1$ (Equation 16) in equation 15 with the specific Rouse number as defined in de Leeuw et al. (2020). This was done to more fairly compare the two methodologies, because de Leeuw et al. (2020) was originally calibrated using

Table 2. List of bed load, suspended sediment entrainment, and total load fluvial sediment transport formulas. We indicate where it was not possible to obtain the equation directly from the original paper due to the lack of access to the paper, language barriers or pay walls. The equations of the publications with a * are used to calculate total transport from a combination of a bed load and suspended sediment entrainment equation.

Bed load transport formulas

Reference	Einstein predictor bed load Φ_b	Comments
Einstein (1942)[α]	$2.1exp^{\frac{-0.391}{\theta}}$	
Meyer-Peter and Müller (1948)	$8(\theta - \theta_{cr})^{1.5}$	0.047 was replaced by θ_{cr}
Meyer-Peter and Müller (1949)[α]	$(4\theta - 0.188)^{1.5}$	
Einstein (1950)[ζ]	$3.97(\theta - \theta_{cr})^{1.5}$	
Bagnold (1966)[ω]	$\frac{e_b u \tau}{(\rho_s - \rho) g \cos S (\tan\phi - \tan S)} / (\sqrt{gRD_{50}^3})$	$e_b = a \log 3.28u + b$ where a and b depend on grain size
K. C. Wilson (1966)[ξ]	$12\theta^{1.5}$	
Ashida and Michiue (1972)[α]	$17(\theta - \theta_{cr})(\sqrt{\theta} - \sqrt{\theta_{cr}})$	0.05 was replaced by θ_{cr}
Fernandez Luque and van Beek (1976)	$5.7(\theta - \theta_{cr})^{1.5}$	
Engelund and Fredsoe (1976)	$5p(\sqrt{\theta} - 0.7\sqrt{\theta_{cr}})$	$p = (1 + (\frac{\frac{\pi}{6}\beta}{\theta - \theta_{cr}})^4)^{-0.25}$, $\beta = 1$ as in Garcia (1991)
Parker (1979)[αω]	$11.2\frac{(\theta-\theta_{cr})^{4.5}}{\theta^3}$	0.03 was replaced by θ_{cr}
Smart (1984)	$4.2S^{0.6}(\frac{u}{u_*})\sqrt{\theta}(\theta - \theta_{cr})$	
van Rijn (1984a)	$0.053D_*^{-0.3}T_0^{2.1}$	$T_0 = \frac{u_*^2 - u_{*cr}^2}{u_{*cr}^2}$
van Rijn (1984a)[ω]	$0.1D_*^{-0.3}S_0^{1.5}$	$S_0 = \frac{\theta - \theta_{cr}}{\theta_{cr}}$
Nielsen (1992)	$12\sqrt{\theta}(\theta - \theta_{cr})$	
Ribberink (1998)	$11(\theta - \theta_{cr})^{1.65}$	
Hunziker and Jaeggi (2002)	$5(\theta - \theta_{cr})^{1.5}$	0.05 was replaced by θ_{cr}
Cheng (2002)	$13\theta^{1.5}exp(-\frac{\theta_{cr}}{\theta^{1.5}})$	0.05 was replaced by θ_{cr}
Camenen and Larson (2005)	$12\theta^{1.5}exp(-4.5\frac{\theta_{cr}}{\theta})$	
Wong and Parker (2006)	$4.93(\theta - \theta_{cr})^{1.6}$	0.047 was replaced by θ_{cr}
Wong and Parker (2006)	$3.97(\theta - \theta_{cr})^{1.5}$	0.0495 was replaced by θ_{cr}

Suspended sediment entrainment formulas

Reference	Near-bed reference concentration C_b / Entrainment E_s	Comments
Einstein (1950)	$\frac{1}{23.2}\frac{\Phi_b}{\sqrt{\theta}}$	$a = 2 * D$
Engelund and Fredsoe (1976)	$\frac{0.65}{(1+\lambda^{-1})^3}$	$\lambda = \sqrt{\frac{\theta - \theta_{cr} - (\frac{\pi}{6}\beta p)}{(0.027(R+1)\theta)}}$, $\beta = 1$, $a = 2 * D$
Smith and McLean (1977)	$\frac{0.65 * \gamma S_0}{1 + \gamma S_0}$	$S_0 = \frac{\theta - \theta_{cr}}{\theta_{cr}}$, $\gamma = 0.0024$ as in de Leeuw et al. (2020) , $a = 26.3(\theta - \theta_{cr})D + k_s$
Itakura and Kishi (1980)[σ]	$0.008(\frac{0.14u_*\Omega}{w_s\theta} - 1)$	$\Omega = \frac{\theta}{0.143}(2 + \frac{exp(-A^2)}{\int_A^\infty exp(-z^2)dz}) - 1$, $A = \frac{0.143}{\theta} - 2$, $a = 0.05h$
Celik and Rodi (1984)[σ]	$1.13\frac{C_m}{\int_{0.05}^1 \left((\frac{1-z/h}{z/h})(\frac{0.05}{1-0.05})\right)^P dz/h}$	$C_m = 0.034(1 - \frac{k_s}{h}^{0.06})\frac{u_*^2 u}{gRhw_s}$, $a = 0.05h$
van Rijn (1984b)	$0.015\frac{DS_0^{1.5}}{aD_*^{0.3}}$	$S_0 = \frac{\theta - \theta_{cr}}{\theta_{cr}}$, $a = max(0.01h, k_s)$
Akiyama (1986)[σ]	$3 * 10^{-12}Z^{10}(1 - \frac{Z_c}{Z})$	$Z = \frac{u_*}{w_s}Re_p^{0.5}$, $Z_c = 5$, $a = 0.05h$
Garcia (1991)	$\frac{1.3*10^{-7}Z^5}{1 + \frac{1.3*10^{-7}}{0.3}Z^5}$	$Z = \frac{u_*}{w_s}Re_p^{0.6}$, $a = 0.05h$
McLean (1992)	$\frac{0.065\gamma S_0}{1 + \gamma S_0}$	$S_0 = \frac{\theta - \theta_{cr}}{\theta_{cr}}$, $\gamma = 0.004$, $a = \frac{0.68(\tau/\tau_c r)D}{1 + (0.0204(\ln(100D))^2 + 0.022\ln(100D) + 0.0709)(\tau/\tau_{cr})}$
Wright et al. (2004)	$\frac{7.8*10^{-7}Z^5}{1 + \frac{7.8*10^{-7}}{0.3}Z^5}$	$Z = \frac{u_*}{w_s}Re_p^{0.6}$, $a = 0.05h$
de Leeuw et al. (2020)	$4.74 * 10^{-4}\frac{u_*}{w_s}^{1.77}Fr^{1.18}$	$a = 0.1h$

[α] Equation reported as in Carrillo et al. (2021)
[ζ] Equation reported as in de Leeuw et al. (2020)
[ω] Equation reported as in Kleinhans (2005)
[ξ] Equation reported as in Soulsby and Damgaard (2005)
[σ] Equation reported as in Garcia (1991)

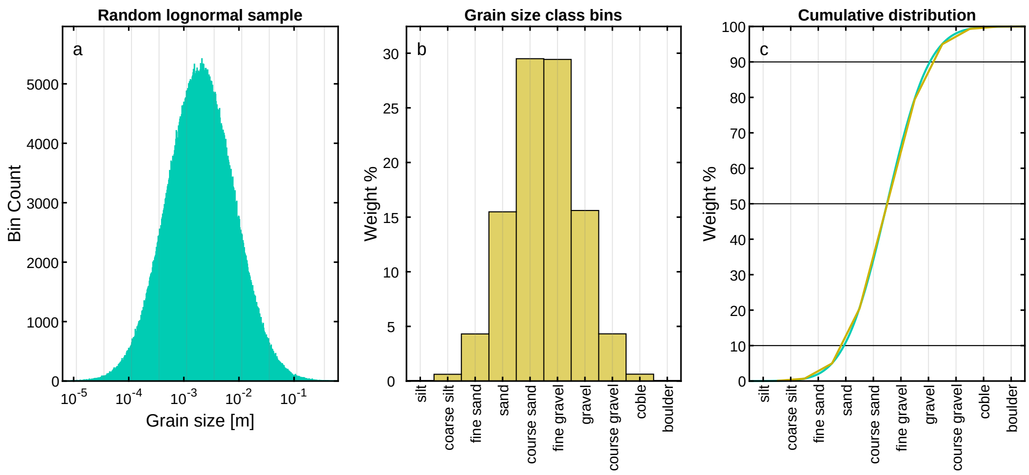

Figure 2. Grain size mixture created from a lognormal grain size distribution (a), divided into grain size classes (b), and visualised as a cumulative distribution (c).

$$\beta = 2.4612 \left(\frac{w_s}{u_*}\right)^{0.547} \tag{21}$$

In addition to analysing transport relations using a single characteristic (or uniform) particle size we also performed calculations explicitly considering the full grain-size distribution of the sediment bed (Fig. 2). The sediment composition is a lognormal distribution with the peak between the coarse sand and fine gravel class (Fig. 2b). The distribution includes sediment fractions from coarse silt to cobles (63 μm–20 cm). The D_{50} of the mixture was used to calculate one Nikuradse bed roughness value, k_s, and one critical Shields number of the mixture, $\theta_{cr,D50}$. Hiding and exposure effects of the mixture were considered by using a function from Parker et al. (1982), so that

$$\theta_{cr,mix} = \theta_{cr,D50} \left(\frac{D_i}{D_{50}}\right)^{-\gamma} \tag{22}$$

where gamma is 0.9 (Parker, 1990) and D_i is the grain size of the sediment fraction of the mixture. A total sediment transport rate was calculated for every sediment class based on the grain size of that class, D_i (replacing D with D_i in equations 8, 10, 14 and 19). We multiplied this rate with the bed fraction of the total sediment composition of that class, $frac_i$, (Fig. 2b). The summation of the transport rates of these classes provide the total sediment transport rate for the mixture. For the calculation of the transport rate of the sediment mixture we only used the equations of total transport previously mentioned (Engelund & Hansen, 1967; de Leeuw et al., 2020).

3 Results

3.1 Effects of gravity on hydraulics

In Figure 3 the effect of gravity is visualised for different calculated hydraulic parameters and a range of input discharges. Figure 3 shows that gravity has clear effects on water depth, hydraulic radius, velocity, shear stress and shear velocity. For a given range of discharges, water depth is inversely correlated with gravity, leading to increased water depth and hydraulic radius on Mars as compared to Earth (Fig. 3a and b). In ad-

Table 3. List of total load fluvial sediment transport formulas.

Total transport formulas Reference	Equations	Comments
Engelund and Hansen (1967)	$q_t = \frac{\Phi_t}{\sqrt{RgD^{3/2}}}$	implicit combination bed and suspended load
	$\Phi_t = \frac{0.1}{f}\theta^{2.5}$	
After de Leeuw et al. (2020)	$q_t = q_b + q_s$	explicit combination bed and suspended load
	$\Phi_b = 5.7(\theta - \theta_{cr})^{1.5}$	Fernandez Luque and van Beek (1976)
	$C_b = \frac{q_b}{h_b u_b}$	
	$u_b = 0.6u,\ h_b = 0.6\left(Fr\left(\frac{D}{h}\right)^2\right)^{0.3}$	
	$q_s = \int_{h_b}^{h} C_b \left(\frac{h-z}{z}\frac{h_b}{h-h_b}\right)^{P_l}$.	
	$\frac{u_*}{\kappa}\ln\left(\frac{z}{z_0}\right) dz$	

Total transport formula for mixtures Reference	Total sediment transport q_t	Comments
	$\sum_{i=1}^{m} frac_i * q_t(D_i)$	i refers to the fractions and m is the number of fractions

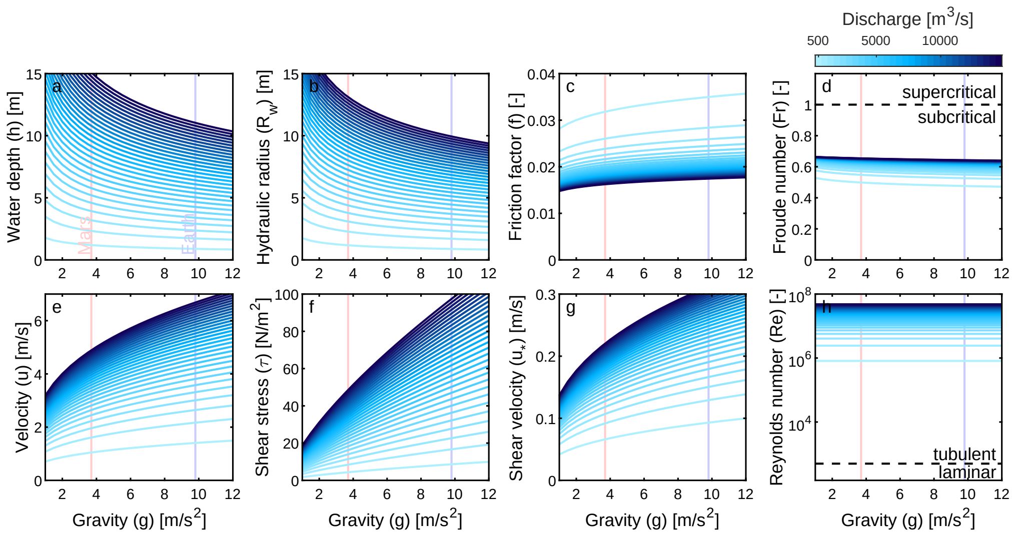

Figure 3. Hydraulic variables calculated using independent variables discharge, slope, and width. (a) Water depth h $[m]$, (b) hydraulic radius R_w $[m]$, (c) friction factor f $[-]$, (d) Froude number Fr $[-]$, (e) velocity u $[m/s]$, (f) shear stress τ $[N/m^2]$, (g) shear velocity u_* $[m/s]$, and (h) Reynolds number Re $[-]$ as a function of gravity g $[m/s^2]$ for a range of discharges Q $[m^3/s]$.

dition, lower gravity reduces velocity, bed shear stress and shear velocity (Fig. 3e–g). The hydraulic parameters are increasingly sensitive to changes in gravity for decreasing gravities. Gravity has no effect on the Reynolds number (Fig. 3h), meaning that the transition from laminar to turbulent flow is independent of gravity for a given discharge. The effect of gravity on the Froude number is existent, but negligible (Fig. 3d). All scenarios considered were subcritical and turbulent.

The effects of gravity are different when water depth is used as independent variable (boundary condition) instead of discharge and are visualised in Figure 4. Since water depth is in this case not dependent on gravity and therefore constant, so is the hydraulic radius (Fig. 4b). Velocity, shear stress, and shear velocity are still strongly af-

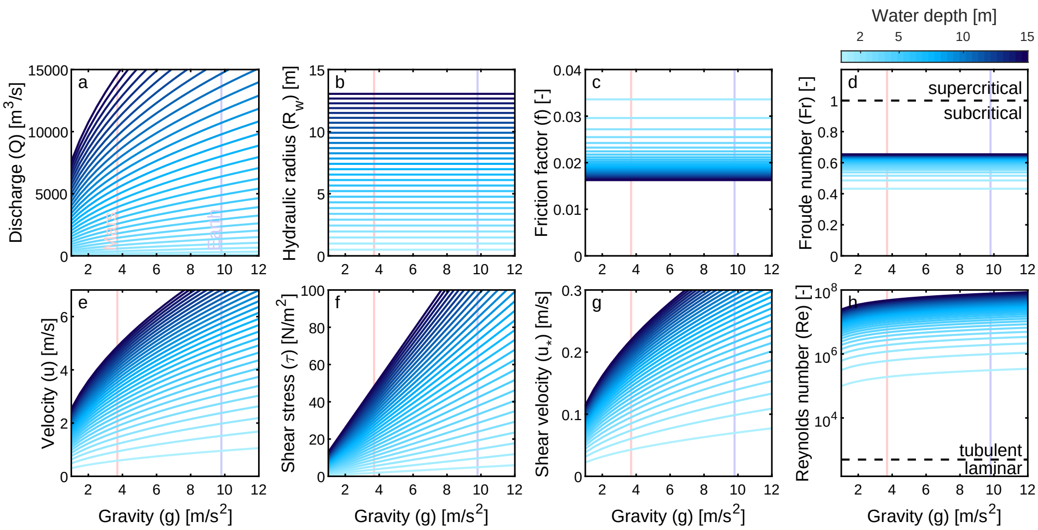

Figure 4. Hydraulic variables calculated using independent variables water depth, slope, and width. (a) Water discharge Q $[m^3/s]$, (b) hydraulic radius R_w $[m]$, (c) friction factor f $[-]$, (d) Froude number Fr $[-]$, (e) velocity u $[m/s]$, (f) shear stress τ $[N/m^2]$, (g) shear velocity u_* $[m/s]$, and (h) Reynolds number Re $[-]$ as a function of gravity g $[m/s^2]$ for a range of water depths h $[m]$.

fected by a change in gravity as is discharge in this case (Fig. 4a, e-g). However, the relation between gravity and shear stress is now linear (Fig. 4f) because there is no gravity component in the water depth, as compared to Figure 3f. The Reynolds number becomes dependent on gravity and the Froude number is no longer dependent on gravity (Fig. 4d and h). The rest of the results presented are based on discharge as independent variable. The effect of gravity on sediment transport with water depth as an independent variable are shown in the Appendix Section A3.

3.2 Effects of gravity on fluvial sediment transport

The response of the hydraulic parameters to changes in gravity in turn affect the transport rate of the sediment. Figure 5 represents the response of settling velocity and sediment mobility to Mars and Earth gravity for a range of grain sizes under a fixed water discharge of 2000 m^3/s. Despite the fact that lower gravity on Mars reduces shear stress and shear velocity (Figure 3; Equation 4), which would decrease fluvial sediment transport rates, the mobility of the sediment increases as a result of two additional mechanisms: Firstly, settling velocity is lower under lower gravity (Fig. 5a; Equation 10), resulting in a lower shear rate for the transition to suspension (Fig. 5b; Equation 9), as noted by previous studies. The settling velocity is independent of the initial hydraulic conditions (i.e., water depth or discharge; Fig. A2a), and depends only on gravity, grain size and relative density. The reduced settling velocity, despite lower martian velocities, increases the transport distance of the grains, as expressed by the advection length (Fig. 5d; Equation 13). Secondly, martian gravity results in a higher Shields number and movability number (Fig. 5b and c; Equation 8) similar to previous findings by Komar (1980), Burr et al. (2006) and Grotzinger et al. (2013), increasing the tendency of the sediment to be mobilised and suspended. This is indicated by the Shields number and Movability number surpassing the thresholds of motion and suspension at larger grain sizes (Fig. 5b and c). As a result, larger grains can be picked up and transported in suspension for martian gravity.

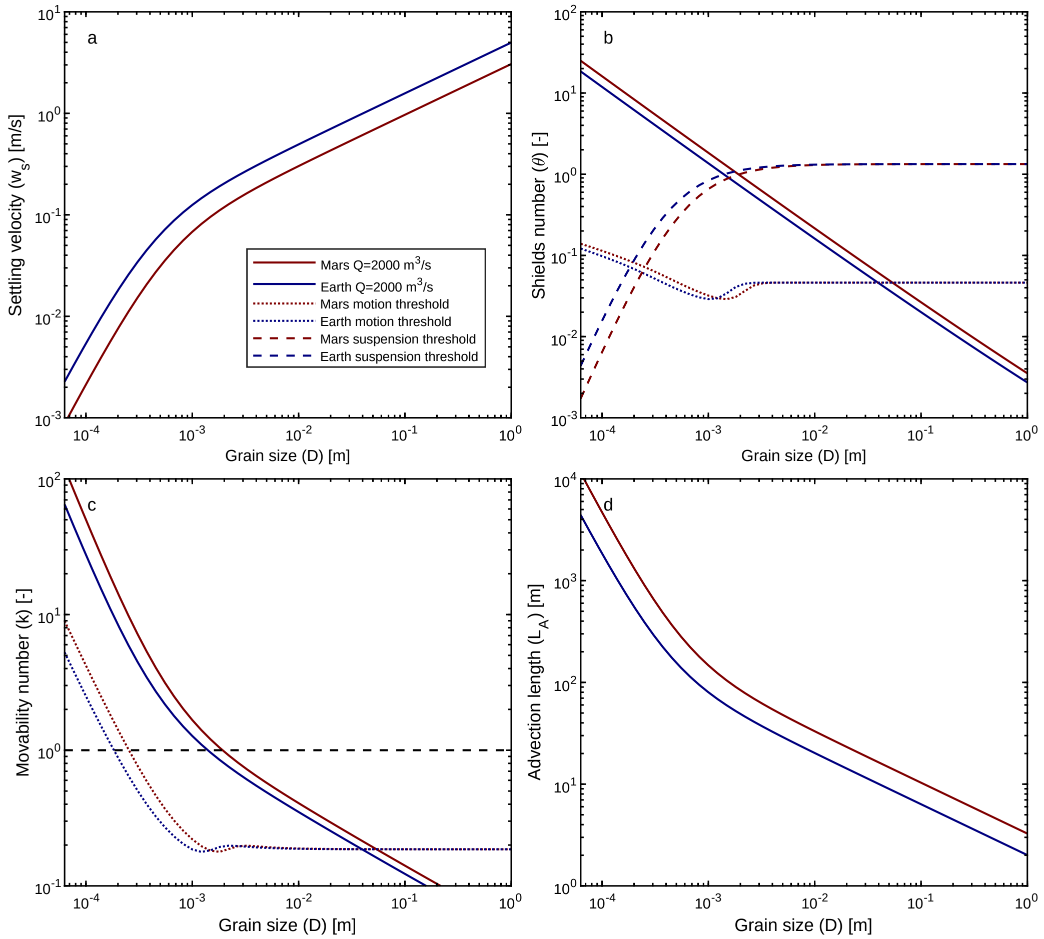

Figure 5. Fluvial sediment transport parameters (a) settling velocity w_s $[m/s]$, (b) Shields number θ $[-]$, (c) movability number k $[-]$, (d) advection length L_A $[m]$ as a function of grain size D_{50} $[m]$ for Mars (red) and Earth (blue) gravitational acceleration g $[m/s^2]$ and a given discharge Q of 2000 m^3/s, where(b and c) include the motion threshold (Zanke, 2003) and suspension threshold ($w_s/u_* = k = 1$). Please note the logarithmic scale in all subplots.

To better understand the effects of gravity on the different modes of transport, we show grain size dependent transport for various transport equations in Figure 6a and b, visualising the equations from Table. 2 using equation 14. Despite the order of magnitude differences in predicted transport rates between different formulas, nearly all equations agree on the relative effect of gravity. The influence of gravity on bed load transport is limited, except for the largest grains that on Earth lie below the threshold of motion (Fig. 6a and c). This bed load transport rate difference is caused by the higher nondimensional shear stress on Mars that results in picking up larger grains for the same discharge (Fig. 5b). Because we consider this a critical effect of gravity, formulas that do not include a critical threshold for mobility are not recommended. They are therefore not included in Figure 6a and c (Einstein, 1942; Meyer-Peter & Müller, 1949; Bagnold, 1966; K. C. Wilson, 1966). Furthermore, a few relations produced smaller bed load transport values towards smaller grain sizes while they should be more easily transported until reaching a maximum concentration. As this seemed undesirable for our purpose, these equations were excluded as well (Engelund & Fredsoe, 1976; van Rijn, 1984a).

The influence of gravity on suspended transport is much stronger than for bed load transport (comparing Fig. 6b with a and d with c). Lower gravity results in more suspended sediment transport. This gravity difference for suspension translates to the total transport per grain size (Fig. 6e). Because suspended sediment is more important for smaller grain sizes, absolute and relative (Fig. 6f), the effect of gravity is stronger for smaller grain sizes. Some suspended transport equations predicted higher suspended transport rates than the bed load transport rate for big grain sizes. They were therefore deemed unsuitable for the purpose of predicting martian transport and not included in Figure 6b and d (Itakura & Kishi, 1980; Celik & Rodi, 1984; Akiyama, 1986; Garcia, 1991; Wright et al., 2004).

By taking the ratio of the total transport of Mars and Earth, the relative differences in transport between Mars and Earth are highlighted for all grain sizes (Fig. 6g). When considering total transport with explicit inclusion of bed load and suspended transport (de Leeuw et al., 2020), the grain sizes at the bed load-suspension transition are affected strongest, leading to a peak of about 3 times higher transport rates for Mars (Fig. 6g). This is because for this grain size range, there is predominantly suspended transport on Mars, whereas bed load transport on Earth. Which sediment class is affected most depends on the flow conditions that define the bed-suspension load transition, which in our scenarios is medium sand. The fine sediments on the left side of the bed load-suspension transition peak are more effected by gravity than the coarse grain sizes on the right side of the peak. This is caused by the higher gravity effect on suspended sediment compared to gravity effect on bed load transport. Nonetheless this gravity effect reduces for silt and smaller grain sizes. This effect is very uncertain as transport equations are often not calibrated for cohesive sediment, i.e., mud ($< 63\mu m$) and is therefore not visualised. For the coarsest grains that are transported, there is a very large peak. This is because these largest grain sizes are only transported as bed load on Mars and not on Earth. No ratio could be determined for transport on Mars without transport on Earth. When these results are compared to the total transport relation that does not distinguish between bed load and suspended transport (Engelund & Hansen, 1967), it is clear that this approach ignores the grain size dependent gravity effect. The relationship provides a transport rate for Mars that is 1.4 times higher than Earth, which is independent of grain size.

3.3 Fluvial sediment transport for a given sediment mixture

Instead of calculating fluvial sediment transport for a uniform, single grain size, the sediment transport rate can also be calculated for a sediment mixture, which is more realistic for natural rivers. For a lognormal sediment distribution (Fig. 2), the total sediment transport rate increases exponentially with decreasing gravity (Fig. 7a). This indicates that the total sediment transport rate for the mixture presented in Figure 2 is

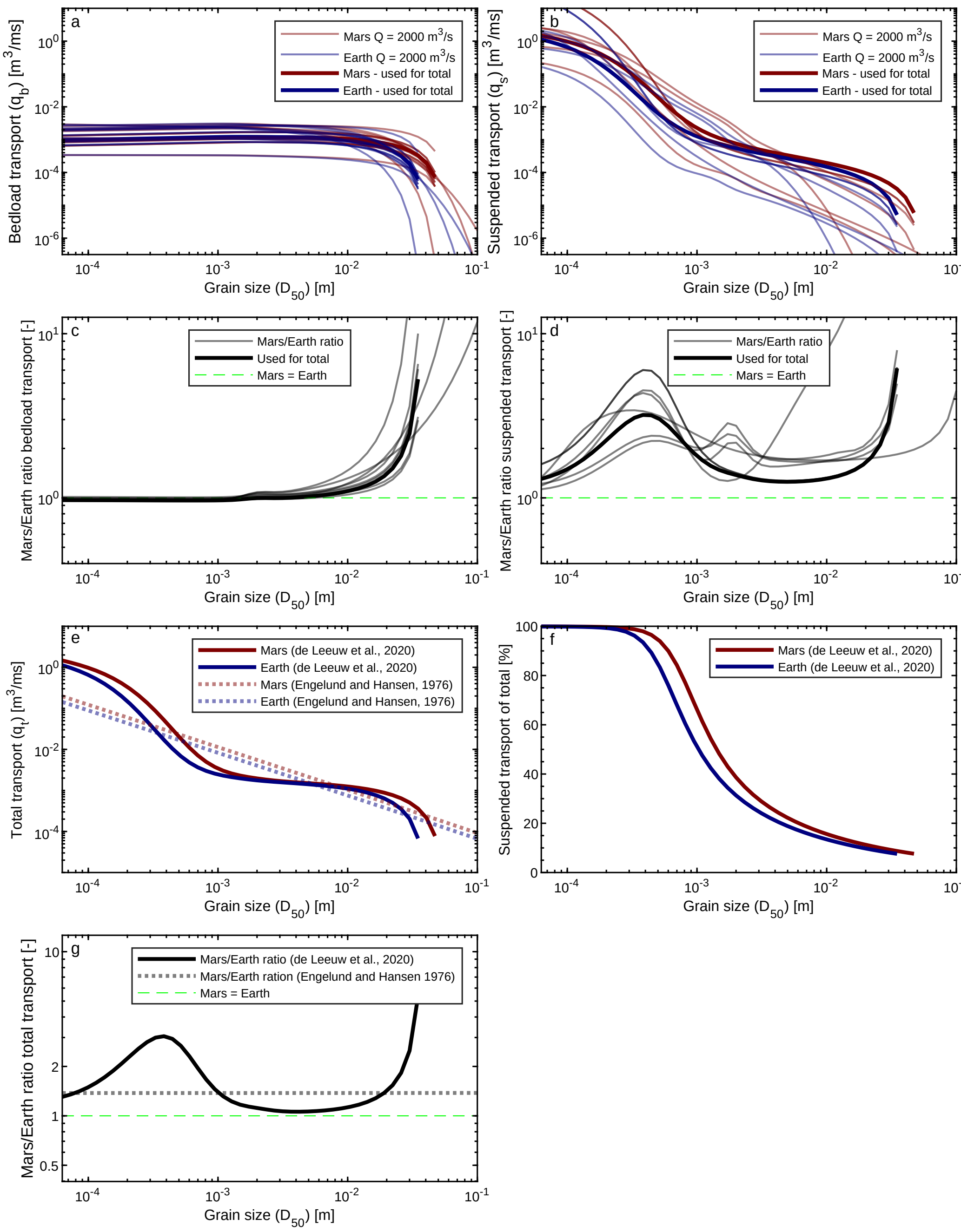

Figure 6. Fluvial transport rates as a function of grain size. (a) Bed load transport rate q_b $[m^3/ms]$ by formulas indicated in Table 2, (b) suspended transport rate q_s $[m^3/ms]$ by formulas indicated in Table 2, (c) bed load transport ratio of Mars and Earth $[-]$, (d) suspended transport ratio of Mars and Earth $[-]$, (e) total sediment transport rate q_t $[m^3/ms]$ by total load equations implicitly (Engelund & Hansen, 1967) and explicitly (de Leeuw et al., 2020) including bed load and suspended transport, (f) percentage of suspended transport of the total sediment transport [%], (g) total transport ratio of Mars and Earth $[-]$, all for Mars (red) and Earth (blue) gravity acceleration g $[m/s^2]$ and a given discharge Q of 2000 m^3/s and channel geometry.

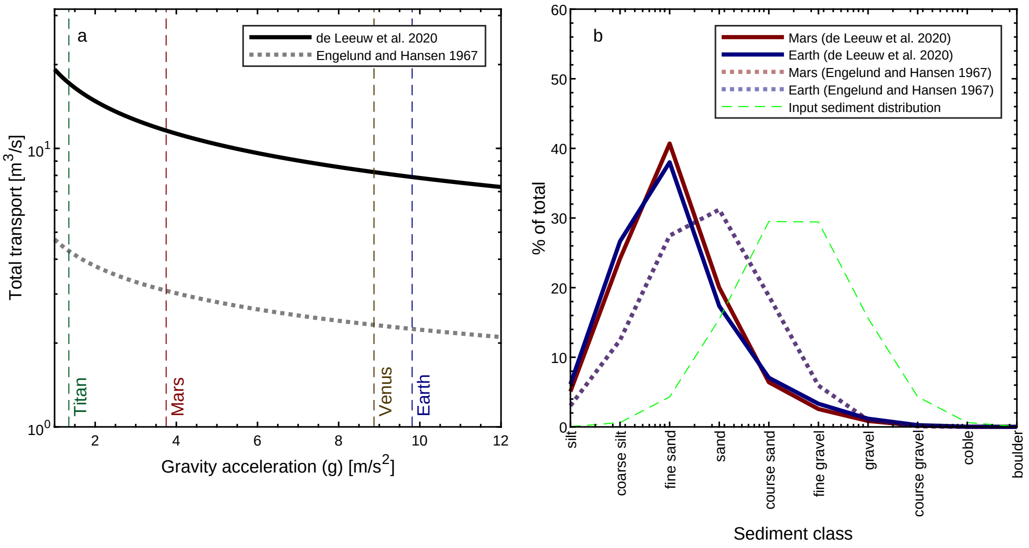

Figure 7. Total fluvial transport rates for the lognormal grain size distribution from Fig. 2 using de Leeuw et al. (2020) and Engelund and Hansen (1967). Each grain size is summed up relative to their fraction of the total load. (a) Total fluvial sediment transport rate q_t $[m^3/ms]$ for a range of gravity g $[m/s^2]$, (b) contribution of each sediment fraction to the total sediment transport rate. Based on independent variables: $Q = 2000m^3/s$, $W = 200m$ and $S = 0.001m/m$.

higher on Mars than Earth. The contribution of different grain size classes to this total value varies slightly between Earth and Mars for the method of de Leeuw et al. (2020): On Mars there is a relatively larger contribution of larger grains (Fig. 7b). The contribution of the grain size classes with the method of Engelund and Hansen (1967) is similar for Earth and Mars as the grain size dependent gravity effect is not included (Fig. 6g). Despite these differences, the total transport of the two methods is comparable in magnitude and shows a similar trend over gravity (Fig. 7a). This is expected as both methods calibrated using the same data.

Figure 7a also indicates the effect of gravity on Titan and Venus. These bodies also have the potential for fluvial transport by a Newtonian fluid. However, these values do not provide much information about the transport rates on Titan and Venus. This study only isolates the effect of gravity, but other differences like fluid and sediment density differences have been ignored. Especially for Titan, this effect is expected to be much larger than the gravity effect.

4 Discussion

4.1 Fluvial sediment transport rates on Mars

Total fluvial sediment transport rates are higher on Mars than on Earth for the same idealised conditions, i.e., water discharge, sediment distribution and channel geometry. This is for two reasons: 1) The threshold for the initiation of motion is lower resulting from a higher Shields number for a given discharge. Consequently, bigger grains are transported, and a smaller discharge is needed on Mars compared to Earth to move sediment and therefore increase transport, non-linearly, after initiation of motion. 2) Relatively more transport occurs in suspension as the larger Shields number shifts the transition zone for bed-suspended load transport towards bigger grain size classes. In addition, the magnitude of suspended transport is higher under lower gravity, which further reduces the ratio between bed load and suspended transport. As a result, net transport rates are higher under lower gravity-conditions, such as on Mars.

Without calculating sediment transport, Komar (1980) and Burr et al. (2006) already showed that martian flows could have transported bigger grain sizes in different transport modes, which they relate to the differences in settling velocity and stream-flow velocity. Furthermore, Amy and Dorrell (2021) identified that suspended sediment flows have a slightly higher potential for transport on Mars, which agrees with our results. In addition, we quantify how the transport modes are affected under martian conditions by calculating bed load and suspended load transport rates separately and as a total rate for a range of grain sizes (Fig. 6). For total load, each grain size experiences larger net transport rates, but fine particles are disproportionally affected because they are more commonly transported as suspension. Consequently, sediment fractions experience gravity differently depending on their transport mode, with important implications for the distribution of grain sizes that are transported and available to deposit.

In this study we isolate the effect of gravity on hydraulics and sediment transport. The model computes capacity-driven transport assuming unlimited sediment availability. However, a freely erodible sediment bed was not only unlikely on Mars due to possible permafrost, but also due to geological constraints like bed armouring (Ferdowsi et al., 2017), cohesive sediment (Braat et al., 2017; van Ledden et al., 2004; Peakall et al., 2007; Edmonds & Slingerland, 2010) and lithological variation (Lamb et al., 2015). Mars used to be more accommodating for fluid water in the Noachian and Early Hesperian, but most likely it has always been cold (Fairén, 2010; Wordsworth, 2016). Ice and permafrost reduce the mobility of channels and enhance overbank deposition (Piliouras et al., 2021), further enhancing relative suspended transport and its effects on morphology. In addition, supply-limited wash load (Khullar, 2007) was likely more significant on Mars than on Earth (Burr et al., 2006; Komar, 1980), though impossible to calculate. Due to the lower suspension threshold and settling velocities (Fig. 5a), a larger portion of the sediments could contribute to the wash load instead of suspended load. Reduced flocculation by lack of organics could have further enhanced this effect (Lee et al., 2017). However, since wash load is not limited by flow, but by supply, a long-term contribution to the sediment load is unlikely.

4.2 Implications for geomorphology and stratigraphy

Because gravity affects fine and coarse sediment fractions differently, we expect differences in morphology and stratigraphy due to varying ratios of sediment fractions and disparities in sediment sorting. Lower gravity reduces settling velocities and increases advection lengths on Mars (Fig. 5), which alters sediment sorting in a standing body of water and longitudinal sorting in decelerating currents (Ferguson & Church, 2004). As a result, we expect coarser bed material on Mars for the same hydraulic and sediment conditions.

The change in ratio between bed load and suspended transport has implications for a range of geomorphological features across scales. Bed load transport affects in-channel morphological development through deposition and erosion, influencing dynamics, height, and the formations and growth of bed forms, point bars and in-channel bars. This 'channel-building' fraction can therefore affect the channel pattern and lateral migration rates. On the other hand, the suspended fraction determines the interaction between the channel and the floodplain. During high flows, sediments are distributed onto the floodplain, influencing floodplain elevation, levee formation, crevasse splays and cut-off infilling. Previous studies on Earth suggested that sand-bed rivers with high suspended loads (like on Mars) promote vertical bar accretion and subsequent conversion to floodplain (Nicholas, 2013). This, in turn, drives the formation of narrower, sinuous channels and reduces channel branching (Nicholas, 2013). As a result of the absolute and relative increase in suspended sediment on Mars, there is an expected higher likelihood of overbank deposit formation during channel flooding with faster and more prominent levee formation. However, it would be difficult to find evidence for this on Mars in the present day due to preferential erosion of the fine overbank deposits (Hayden et al., 2019).

Another consequence of higher suspension rates is an increased chance of hyperconcentrated flows (Burr et al., 2006; Komar, 1980), especially if fine sediment was abundantly present. Flows on Mars likely carried more sediment and were therefore possibly more erosive (also suggested by Bagnold (1962)). When entering a standing water body, these flows can create stratification or density-driven flows due to density differences, resulting in a higher likelihood of turbidity currents and deposits on Mars. In addition, we expect that larger suspended sediment fractions in deltas lead to deeper channels, less reworking, and a rugose delta brink contour, both with and without cohesivity (van der Vegt et al., 2016). Furthermore, we expect lower depositional slopes, due to the settling of particles over a longer distance (longer advection length due to reduced settling velocities) transporting more sediment to the delta front and the prodelta (van der Vegt et al., 2016). This may impact the slopes of delta foresets in stratigraphy, which is important for missions aiming to take sediment samples in the search for biosignatures (Vago et al., 2017). In contrast, (Konsoer et al., 2018) state that suspended dominated flows on Mars require steeper slopes to produce the same bed shear stress and move sediment, all other things being equal. This is true for martian turbidity currents and shear stresses, however, the grains also weigh less which results in enhanced sediment transport in alluvial channels and reduced settling over larger distances, causing lower depositional slopes.

Lastly, the largest effect of gravity on geomorphology is caused by the higher total transport rate on Mars, which suggest that depositional landforms developed faster than their counterparts on Earth for the same discharge. As the fluvial sediment transport rate could be several times greater (e.g. 3 times higher for medium sand; Fig. 5; or 50% higher based on the chosen mixture; Fig. 6), fluvial alluvial landforms visible on Mars would have required a shorter period of fluvial activity to form compared to Earth. In other words, over the same time period, the same discharge would develop a much larger landform on Mars. Yet, the temporal variability of fluvial sediment transport is large. It has been argued that the intermittency factor, defined as the fraction of total time in which bankfull flow would accomplish the same amount of sediment transport as the real hydrograph, is much smaller on Mars (Hayden et al., 2019). This could result in longer fluvial activity for landforms on Mars despite transport being more efficient.

4.3 Best practice for planetary fluvial sediment transport calculations

Our model can be used to estimate past fluvial sediment transport for typical martian channels, when channel geometry, grain size and one hydraulic parameter are available. In theory, the geometry of the channel can be obtained from stratigraphy or channel remnants at the surface. However, obtaining accurate channel geometry is challenging due to alterations over time and limited detailed elevation data. In this study, discharge is used as the hydraulic parameter, although water depth (see Appendix), which can be estimated from features like river terraces, may be more feasible. Given the high uncertainty in these parameters, it is recommended to utilize upper and lower estimates and run multiple model scenarios to obtain a range of martian sediment transport.

Fluvial sediment transport equations are semi-empirical equations that are fitted to physical experiments or field data obtained on Earth. As the equations are physics-based, we assume the relations between gravity and sediment transport is the same on Earth and Mars, despite that the empirical part of equations might not capture martian conditions accurately. However, it is practically impossible to conduct physical experiments under reduced gravity conditions for long enough time periods to represent realistic sediment transport rates. For example, drop tower experiments take about 5 seconds each and parabolic flights 30 seconds. In addition, more physical reliable models using the discrete element method (DEM) using computational fluid mechanics (CDF) (e.g., Schmeeckle, 2014), in which the movement of individual grains are modelled, are extremely computationally expensive. Consequently, analytical, and numerical models can help to evaluate existing transport laws and provide estimates of transport rates on other planets. Although there is a risk that gravity might be hidden in some of the coefficients, past experiments testing different sediment densities in combination with non-dimensional analysis have helped addressing potential biases (Kleinhans, 2005).

We recommend using a total load equation that explicitly defines a relation for bed load and suspended load transport. By using a simplified total load equation that does not distinguish between transport modes, important effects of gravity on sediment transport are overlooked. Considering all formulas discussed, though more options are available, we recommend the method of de Leeuw et al. (2020) using bedload-layer equations as this approach is the most recent study to the authors knowledge that explicitly combines bed load and suspended transport. The approach is valid for a broad range of grain sizes and is well calibrated and validated. We want to emphasize that this is our recommendation for Mars. Most formulas are designed with a specific purpose in mind for Earth (e.g., gravel bed rivers) and could therefore be a better choice for a specific location on Earth. Figure 6a and b could contribute to modellers picking the most suitable equation for their own research.

The equation of Engelund and Hansen (1967) is a popular equation in terrestrial fluvial geomorphology because it is simple and predicts the correct order of magnitude of sediment transport. It is a popular equation in 2D horizontal models because it creates realistic channel patterns (Baar et al., 2019). However, since our results have shown that gravity acts differently on suspended sediment compared to bed load transport, total load equations that are calibrated for Earth and do not separate these modes of transport should be avoided in case of Mars. Figure 6e and g include the total load equation from Engelund and Hansen (1967), with which all grain sizes are affected uniformly by gravity (Fig. 6g). This leads to a different sediment distribution being transported (Fig. 7b), despite that the total transport rate seems similar to the method explicitly combining bed and suspended load (Fig. 7a). First, Engelund and Hansen (1967) do not account for a strong increase in transport for the grains sizes that pass the threshold from bed load to suspended load for lower gravity. Second, the suspended load should increase relatively to the bed load transport in total and for all grain sizes for lower gravity. Third, the equation of Engelund and Hansen (1967) does not account for a critical shear stress, a non-negligible factor.

Finally, we stress to clearly describe your independent variables, i.e., input conditions. As shown in Figure 8a–b and the Appendix, a water level boundary can lead to completely different conclusions on the fluvial sediment transport comparison between Earth and Mars compared to results with a discharge boundary. Aside from discharge and water level, one could also input velocity or bed shear stress as their independent variable (Fig. 8). Though it is shown here that transport on Mars is higher for equal discharge, velocity, and shear stress, but not water depth (Fig. 8), different input conditions can lead to different conclusions. Especially the grain size mixture can alter the trends, as different grain sizes experience a different effect of gravity (Figure 6g). The choice of input conditions will depend on the data availability and the research question.

4.4 Application to other planets and moons

The focus of this research has been on defining differences in fluvial sediment transport between Earth and Mars. However, these results can also be valuable to calculate

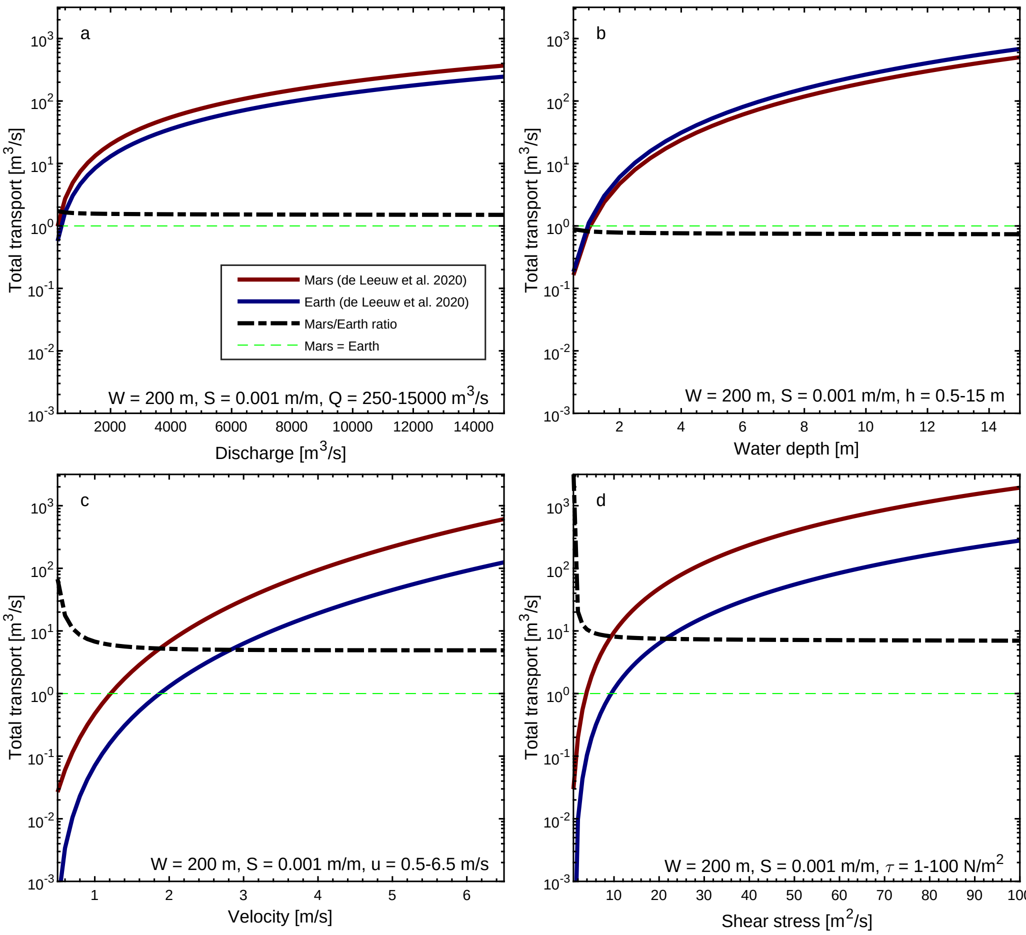

Figure 8. Total fluvial transport rates for different independent variables (i.e., boundary conditions, i.e., input conditions) related to flow. Total sediment transport rate q_t $[m^3/ms]$ for a range of (a) discharges Q $[m^3/s]$ (original settings), (b) flow depths h $[m]$ (Appendix), (c) velocities u $[m/s]$, (d) shear stresses τ $[m^2/s]$. All transport rates are based on Einstein (1950) and the sediment mixture (Fig. 2).

sediment transport on other planetary bodies or moons with significant Newtonian surface liquid (Fig. 7a). Titan is an obvious target, as Titan has a hydrocarbon cycle in which liquid methane and ethane flow like a liquid at the surface. Images from the imaging Subsystem (ISS) (Porco et al., 2004) and Visual and Infrared Mapping Spectrometer (VIMS) (Brown et al., 2004) aboard the Cassini-Huygens mission have shown erosional and depositional landforms (Nixon et al., 2018) including alluvial fans (Birch et al., 2016), active river deltas (Wall et al., 2010), and river valleys (e.g., Burr et al., 2013). The gravity effect for Titan can be obtained from this study (Fig. 3 and 7a), however, there is also a significant effect of sediment and fluid density that adds to transport differences that are not considered here. Previous authors (Witek & Czechowski, 2015; Burr et al., 2006) already showed that transport, and especially suspended transport, in rivers on Titan is more effective than in terrestrial rivers for the same discharge, similar to results we observed for Mars. Potential future work is to analyse combined density and gravity effects on fluvial sediment transport with our parameterised model with the aim to interpret data from Titan.

Channels have also been identified on Venus that could be attributed to ancient fluvial activity (Khawja et al., 2020). Nonetheless, it is still highly uncertain if the climate on early Venus was similar enough to Earth to allow liquid water at the surface. Resolution of surface features at decametre scales on Venus shall be enabled by VenSAR (a phased array synthetic aperture radar) (Ghail et al., 2018) aboard ESA's EnVision mission, currently scheduled for launch in 2031. EnVision, and future missions observing the Venusian surface will provide data to which the approach of this paper could be applied. Our model could be used to investigate channel dimensions and sediment transport rates on Venus when more data is available, to estimate if the channels were formed by a Newtonian fluid (possibly water) or not (likely lava). If the fluid shaping the channels was water, hydraulic and sediment transport processes would be remarkably similar to Earth, because the difference in gravity between Earth and Venus is relatively small (Fig. 7a).

5 Conclusion

This study aimed to isolate and clarify the effect of gravity on fluvial sediment transport in an open, single-thread, alluvial channel for transport capacity limited, unidirectional, steady uniform flow. By using an analytical model, we compared a scenario with fixed channel geometry and discharge for Earth and Mars gravity to: 1) test the response of hydraulic and associated sediment transport parameters; 2) estimate total sediment transport for a range of sediment grain sizes and a mixed sediment distribution; 3) compile, compare, and test the suitability of a range of sediment transport equations for application on Mars. We conclude that, because of the smaller force pulling the water downslope on Mars, the velocity and bed stresses are lower and water depth is higher for the same discharge. Despite this effect on the hydraulics, the mobility of the sediment is higher on Mars because particle weight is reduced due to lower gravity. The results showed that bigger grains can be entrained and suspended. Furthermore, the suspended transport rate is higher for lower gravity, while the bed load transport is less effected. Therefore, the total sediment transport rate is higher for the same discharge on Mars and the relative contribution of suspended sediment is higher. Because the effect of gravity is different for bed load and suspended load, the effect of gravity varies with grain size and is expected to impact morphology and stratigraphy. Likely effects are increased overbank sedimentation processed and reduced in-channel processes. Lastly, we advise to avoid using total load formulas for Mars, because they ignore that the effect of gravity varies with transport mode. Our results stress the significance of gravity on hydraulic and sedimentary processes and provide new insights into Earth-derived fluvial sediment transport formulas for estimating transport rates and morphological change on Mars and other planets and moons.

Appendix A

A1 Thresholds for the initiation of motion

In this study we considered 18 equations for the initiation of motion of 16 publications (Table A1). In Figure A1 we plotted the traditional equations of Brownlie (1981) and Soulsby (1997) and added less common equations of Mantz (1977) as described in Komar and Clemens (1986) and Paphitis (2001) and their own equations. From Paphitis (2001) we plotted two different equations and from Komar and Clemens (1986) we used their more generalised form of Collins and Rigler (1982). Because this equation was most reliable, we did not use any of the other equations mentioned in Komar and Clemens (1986) or Collins and Rigler (1982). The Soulsby (1997) equation is sometimes also cited as Soulsby and Whitehouse (1997) and is for example used in Kleinhans et al. (2017) and Lapôtre and Ielpi (2020). Additionally, we plotted more modern equations of the initiation of motion from Zanke (2003), Cao et al. (2006), van Rijn (2007) and Simões (2014).

In addition to the equation in the plot we also considered the Zanke (2003) fit from Kleinhans (2005) but was discarded because of the limited grain size range compared to the original Zanke (2003). We discovered that citation of Brownlie (1981) in Miedema (2010) and Righetti and Lucarelli (2007) seemed incorrectly cited. The equation differed from the original and the dimensional critical shear stress seemed to increase incorrectly for smaller grain sizes. A similar trend was observed with the equation from Beheshti and Ataie-Ashtiani (2008) and was therefore discarded.

After these considerations, the remaining 10 equations were all very similar (Fig. A1). The largest differences occur in the cohesive regime. One equation deviates significantly from the other equations, which is the equation from Simões (2014). In the main part of the paper, we used Zanke (2003) (visible in green), because this equation is most physics-based, while many other equations are empirical fits to flume data, which could contain hidden gravity components in the coefficients. In addition, this equation has the advantage that it is valid for all grain sizes, while the empirical fits are only valid for a specific grain size range.

The following equations are used to calculate the initiation of motion by Zanke (2003).

$$\theta_{cr} = \frac{(1-n) \cdot tan(\phi/1.5) \cdot K}{\left(1 + 1.8 \cdot \frac{u'_{rms,b}}{u_b}\right)^2 \cdot \left(1 + 0.4\left(1.8 \cdot \frac{u'_{rms,b}}{u_*}\right)^2 \cdot tan(\phi/1.5) \cdot K\right)} \tag{A1}$$

where ϕ is the angle of repose, n the porosity fraction, K is a parameter for the cohesive effect, u_b is the time-averaged flow velocity acting on the grain, u_* is the shear velocity and $u'_{rms,b}$ is the standard deviation of the velocity fluctuation.

$$K = 1 + \frac{3e-8}{(\rho_s - \rho) * D^2} \tag{A2}$$

$$\frac{u'_{rms,b}}{u_*} = 0.31 R_e^* \cdot e^{-0.1 R_e^*} + 1.8 e^{-0.88 \frac{D}{h}} \cdot (1 - e^{-0.1 R_e^*}) \tag{A3}$$

$$\frac{u'_{rms,b}}{u_b} = \frac{u'_{rms,b}/u_*}{u_b/u_*} \tag{A4}$$

$$\frac{u_b}{u_*} = 0.8 + 0.9 \frac{u_y}{u_*} \tag{A5}$$

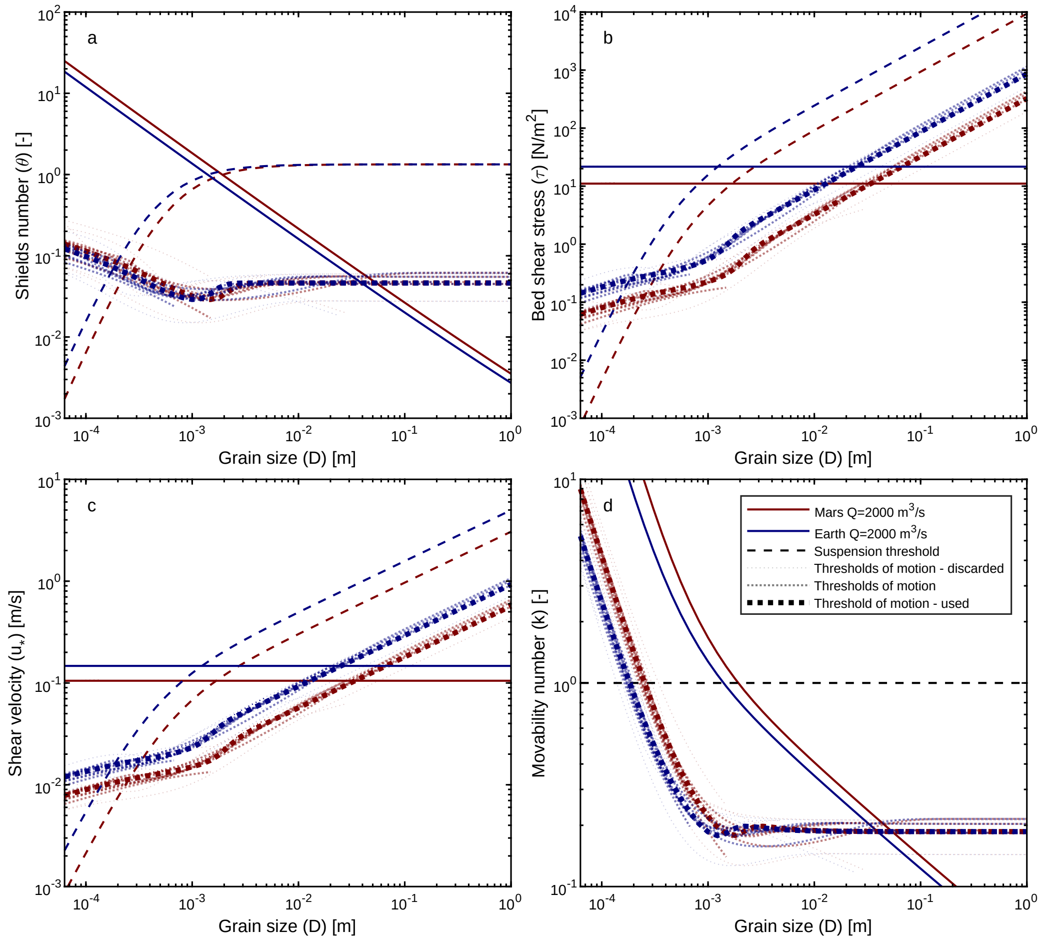

Figure A1. Mobility and suspension thresholds for (a) Shields number, i.e. nondimensional shear stress θ $[-]$, (b) bed shear stress τ $[N/m^2]$, (c) shear velocity u_* $[m/s]$ and (d) movability number k $[-]$ as a function of grain size for a given discharge Q $[m^3/s]$ and two gravities g of 3.7 and 9.8 m/s^2.

$$\frac{u_y}{u_*} = \left(\frac{1 - P_t}{R_e^{*2}} + \frac{P_t}{(2.5ln(1) + B)^2} \right)^{-0.5}; \tag{A6}$$

$$B = (1 - P_t) \cdot (2.5 \ln(R_e^* + 5.25) + 8.5P_t \tag{A7}$$

$$P_t = 1 - e^{-0.08R_e^*} \tag{A8}$$

$$R_e^* = \frac{Du_*}{\nu} \tag{A9}$$

A2 Selection of bed load and entrainment relations

Considering all cited bed load transport relations (Table 2), we recommend using a bed load equation that includes a critical value for mobility. Some equations are more

Table A1. Curves for the initiation of motion

Critical Shields curves		
Mantz (1977) as in Komar and Clemens (1986) and Paphitis (2001)	$\theta_{cr} = 0.1Re_*^{-0.3}$	Fig. A1
Brownlie (1981)	$\theta_{cr} = 0.22Re_p^{-0.6} + 0.06 * 10^{-7.7Re_p^{-0.6}}$	Fig. A1
Brownlie (1981) as in Miedema (2010) and Righetti and Lucarelli (2007)	$\theta_{cr} = 0.22Re_p^{-0.9} + 0.06exp(-17.77 * Re_p^{-0.9})$	discarded
Soulsby (1997) / Soulsby and Whitehouse (1997)	$\theta_{cr} = \frac{0.3}{1+1.2D_*} + 0.055(1 - exp(-0.02D_*))$	Fig. A1
Soulsby (1997) / Soulsby and Whitehouse (1997) as in Kleinhans et al. (2017)	$\theta_{cr} = 0.5(\frac{0.3}{1+1.2D_*} + 0.055(1 - exp(-0.02D_*)))$	discarded
Paphitis (2001)	$\theta_{cr} = \frac{0.188}{1+Re_*} + 0.0475(1 - 0.699exp(-0.015 * Re_*))$	Fig. A1
Paphitis (2001)	$\theta_{cr} = \frac{0.273}{1+1.2D_*} + 0.046(1 - 0.576exp(-0.02 * D_*))$	Fig. A1
Zanke (2003)	$\theta_{cr} = \frac{(1-n)\cdot tan(\phi/1.5)\cdot K}{\left(1+1.8\cdot\frac{u'_{rms,b}}{u_b}\right)^2\cdot\left(1+0.4\left(1.8\cdot\frac{u'_{rms,b}}{u_*}\right)^2\cdot tan(\phi/1.5)\cdot K\right)}$	Main paper; Fig. A1
Zanke (2003) fit from Kleinhans (2005)	$\theta_{cr} = 0.145Re_p^{-0.33} + 0.045 * 10^{-1100Re_p^{-1.5}}$	discarded
Cao et al. (2006)	$Re_p < 6.61 \Rightarrow \theta_{cr} = 0.1414Re_p^{-0.2306}$ $6.61 \leq Re_p \leq 282.84 \Rightarrow$ $\theta_{cr} = (1 + (0.0223Re_p)^{2.8358})^{\frac{0.3542}{3.0946Rep^{0.6769}}}$ $Re_p > 282.84 \Rightarrow \theta_{cr} = 0.045$	Fig. A1
van Rijn (2007)	$D_* < 4 \Rightarrow \theta_{cr} = 0.115D_*^{-0.5}$ $4 \leq D_* < 10 \Rightarrow \theta_{cr} = 0.14D_*^{-0.64}$	Fig. A1
Critical movability curves		
Komar and Clemens (1986)	$k_{cr} = 1.8Re_*^{-1.3}$	discarded
Komar and Clemens (1986)	$k_{cr} = 1.14Re_*^{-1.37}$	discarded
Komar and Clemens (1986)	$k_{cr} = 5.54Re_p^{-1.09}$	discarded
Beheshti and Ataie-Ashtiani (2008)	$0.4 < D_* \leq 10 \Rightarrow k_{cr} = 9.6674D_*^{-1.57}$ $10 < D_* < 500 \Rightarrow k_{cr} = 0.4738D_*^{-0.226}$	discarded
Simões (2014)	$k_{cr} = 0.215 + \frac{6.79}{D_*^{1.7}} - (0.075exp(-2.62 * 10^{-3D_*}))$	Fig. A1
Critical shear stress curves		
Collins and Rigler (1982)	$\tau_{cr} = 1.24w_s^{0.33}$	discarded
Critical shear velocity curves		
Komar and Clemens (1986) after Collins and Rigler (1982)	$u_{*,cr} = 0.482(Rg\nu)^{0.282}w_s^{0.154}$	Fig. A1

useful than others as many formulas are developed with a single purpose in mind, for example just for coarse-grained rivers. Also, very few studies investigated combined bed load and suspended load transport (e.g., Einstein, 1950; Engelund & Fredsoe, 1976; van Rijn, 1984a, 1984b; de Leeuw et al., 2020). Because the thresholds for motion and suspension differ on Mars, we prefer equations that contain a critical value for mobility (Meyer-Peter & Müller, 1948; Einstein, 1950; Ashida & Michiue, 1972; Fernandez Luque & van Beek, 1976; Engelund & Fredsoe, 1976; Parker, 1979; Smart, 1984; van Rijn, 1984a; Nielsen, 1992; Ribberink, 1998; Hunziker & Jaeggi, 2002; Cheng, 2002; Camenen & Larson, 2005; Wong & Parker, 2006). Equations that are therefore not recommended for Mars are Einstein (1942), Meyer-Peter and Müller (1949), Bagnold (1966) and K. C. Wilson (1966) and not plotted in Figure 6a and c. It should be noted that while Camenen and Larson (2005) and Cheng (2002) use a critical value, these equations do not cut off the transport at large grain sizes but use an exponential reduction in transport related to the critical Shield's curve. Meyer-Peter and Müller (1949) does not use a realistic critical Shields value but does have a cut off. A few equations unexpectedly decrease in bed load transport for smaller grain sizes (Einstein, 1942; Engelund & Fredsoe, 1976; van Rijn, 1984a). This is slightly counter intuitive and are therefore also not included in Figure 6a and c. A few equations deviate from the majority without specific reason (van Rijn, 1984a; Smart, 1984), it is unclear how dependable these equations are. Many of the bed load equations are consistent, predictable, and therefore reliable results are mostly of the form $A(\theta - \theta_{cr})^B$, many modelled after Meyer-Peter and Müller (1948).

Suspended sediment entrainment relations show more variation than bed load equations. The formula from Itakura and Kishi (1980) is not valid for all grain sizes and is therefore not useful for our purpose. In addition, the formulas from Celik and Rodi (1984), Akiyama (1986), Garcia (1991) and Wright et al. (2004) show transport rates that are too high for large grain sizes, because the values are higher than all bed load transport formulas and pass the no motion threshold. These equations are also deemed unsuitable for this purpose and therefore not visualised (Fig. 6b and d).

A3 Fluvial sediment transport for a given water depth

In contrast to the results discussed in the main body of the paper, the following fluvial sediment transport results are based on a given water depth rather than a given water discharge. Meaning that the water depth between the Earth and Mars scenario is the same and no longer gravity dependent. We have already seen from Figure 4 that therefore the hydraulic radius and the Froude number are not gravity dependent. In addition, the relation between shear stress and gravity is in this case a simple linear relation. Consequently, the sediment transport parameters and rate differ as well. The non-dimensional shear stress is no longer depended on gravity, meaning that for the same water depth, Mars and Earth can transport the same grain sizes (Fig. A2b and c). For the suspension threshold there is a difference, but it is very minor. The movability number and the advection length only show higher numbers for Mars for smaller grain sizes. The effect of gravity on movability and advection length does not exist for coarse grains for a given water depth. Again, this stresses that grain sizes are affected differently by gravity.

For a given water depth there is more bed load transport on Earth compared to Mars (Fig. A3a). The effect of gravity on suspended load is more complicated (Fig. A3b). The suspended sediment entrainment equations do not all show the same relation. A general trend can be extracted. For median grain sizes (sands), the suspended transport on Mars is a bit higher, while for fine grain sizes (clay/silt), most equations predict that transport on Earth is slightly higher or equal. The effect on the coarse grain sizes (gravel/cobbles/boulders) is less important because those are dominated by bed load transport. In total will still see that more sediment is transported in suspension on Mars for a given water depth (Fig. A3d), similar as for a given discharge (Fig. 6d). This mostly impacts the grain sizes at the bed-

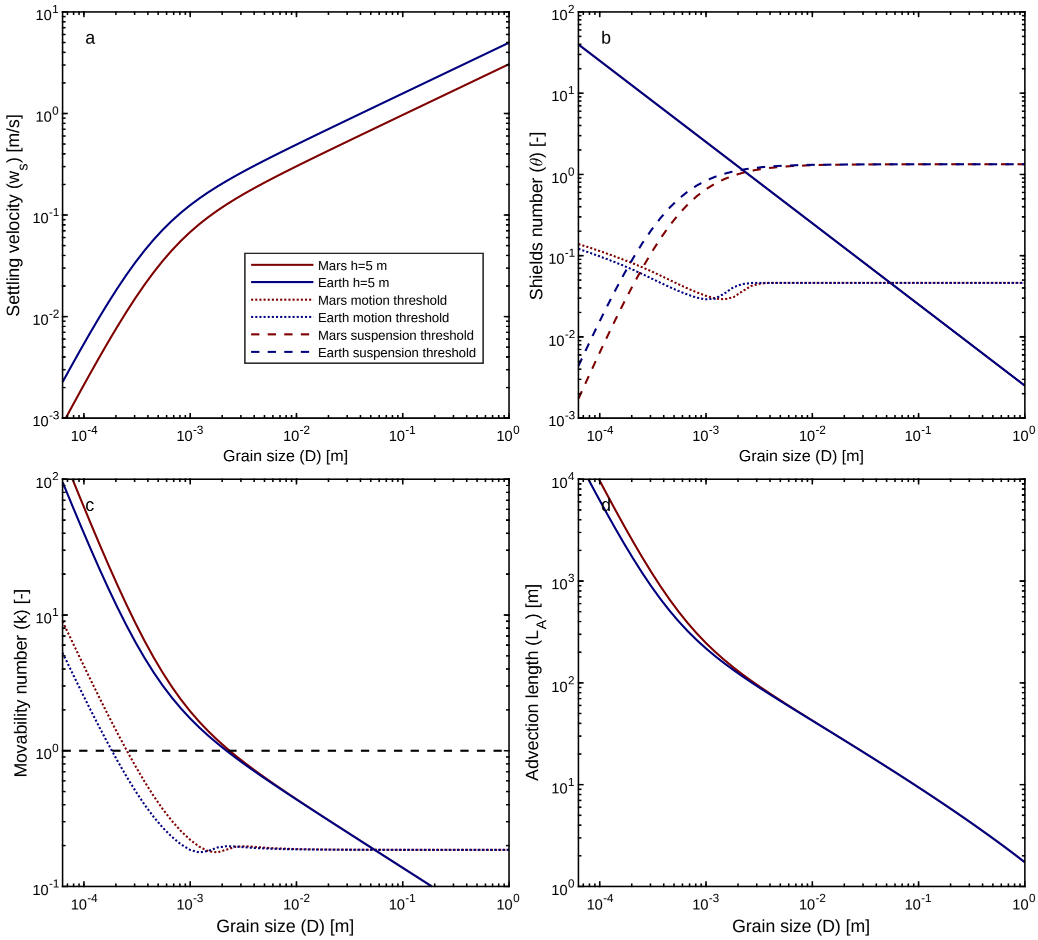

Figure A2. Fluvial sediment transport parameters (a) settling velocity w_s $[m/s]$, (b) Shields number θ $[-]$, (c) movability number k $[-]$, (d) advection length L_A $[m]$ as a function of grain size D_50 $[m]$ for Mars (red) and Earth (blue) gravity acceleration g $[m/s^2]$ and a given water depth h $[m]$. Please note the logarithmic scale in all subplots.

suspended load boundary. However, looking at the Mars/Earth total transport ratio, it is clear that in general (fine and coarse grains) the transport on Mars is lower for a giver water depth (Fig. A3e). Nonetheless, the sands are still transported more efficiently on Mars. The net effect on transport will therefore depend on the sediment composition of the bed.

Open Research

No data was used in this paper. The analytical model and visualisation scripts are available via GitHub and are permanently available via Zenodo (Braat, 2023). For this analysis, MATLAB version R2022b was used.

Acknowledgments

This research was funded by a Rubicon fellowship (019.192EN.009) from the Dutch Research Council (NWO) and a Research Fellowship from the European Space Agency (ESA) awarded to Lisanne Braat. We like to thank Sinéad Lyster and an anonymous reviewer for their valuable comments that helped improve the manuscript.

References

Akiyama, J. (1986). Entrainment of non cohesive sediment into suspension. In *Proc. 3rd int. symp. on river sedimentation, 1986* (pp. 804–813).

Amy, L., & Dorrell, R. (2021). Equilibrium sediment transport, grade and discharge for suspended-load-dominated flows on Earth, Mars and Titan. *Icarus*, *360*(15), 114243. doi: 10.1016/j.icarus.2020.114243

Ashida, K., & Michiue, M. (1972). Study on hydraulic resistance and bed-load transport rate in alluvial streams. In *Proceedings of the japan society of civil engineers* (Vol. 1972, pp. 59–69).

Baar, A., Boechat Albernaz, M., van Dijk, W., & Kleinhans, M. (2019). Critical dependence of morphodynamic models of fluvial and tidal systems on empirical downslope sediment transport. *Nature communications*, *10*(1), 1–12. doi: 10.1038/s41467-019-12753-x

Bagnold, R. A. (1962). Auto-suspension of transported sediment; turbidity currents. *Proceedings of the Royal Society of London. Series A. Mathematical and Physical Sciences*, *265*(1322), 315-319. doi: 10.1098/rspa.1962.0012

Bagnold, R. A. (1966). *An approach to the sediment transport problem from general physics*. US government printing office.

Bahia, R. S., Covey-Crump, S., Jones, M. A., & Mitchell, N. (2022). Discordance analysis on a high-resolution valley network map of mars: Assessing the effects of scale on the conformity of valley orientation and surface slope direction. *Icarus*, *383*, 115041. doi: 10.1016/j.icarus.2022.115041

Baker, V. R., & Milton, D. J. (1974). Erosion by catastrophic floods on Mars and Earth. *Icarus*, *23*(1), 27-41. doi: 10.1016/0019-1035(74)90101-8

Beheshti, A. A., & Ataie-Ashtiani, B. (2008). Analysis of threshold and incipient conditions for sediment movement. *Coastal Engineering*, *55*(5), 423-430. doi: 10.1016/j.coastaleng.2008.01.003

Birch, S., Hayes, A., Howard, A., Moore, J., & Radebaugh, J. (2016). Alluvial fan morphology, distribution and formation on titan. *Icarus*, *270*, 238–247. doi: 10.1016/j.icarus.2016.02.013

Braat, L. (2023). *Planetary-fluvial-sediment-transport-model: Paper final (version v3)*. `https://doi.org/10.5281/zenodo.8056355`. GitHub repository. doi: 10.5281/zenodo.8056355

Braat, L., van Kessel, T., Leuven, J. R., & Kleinhans, M. G. (2017). Effects of mud supply on large-scale estuary morphology and development over

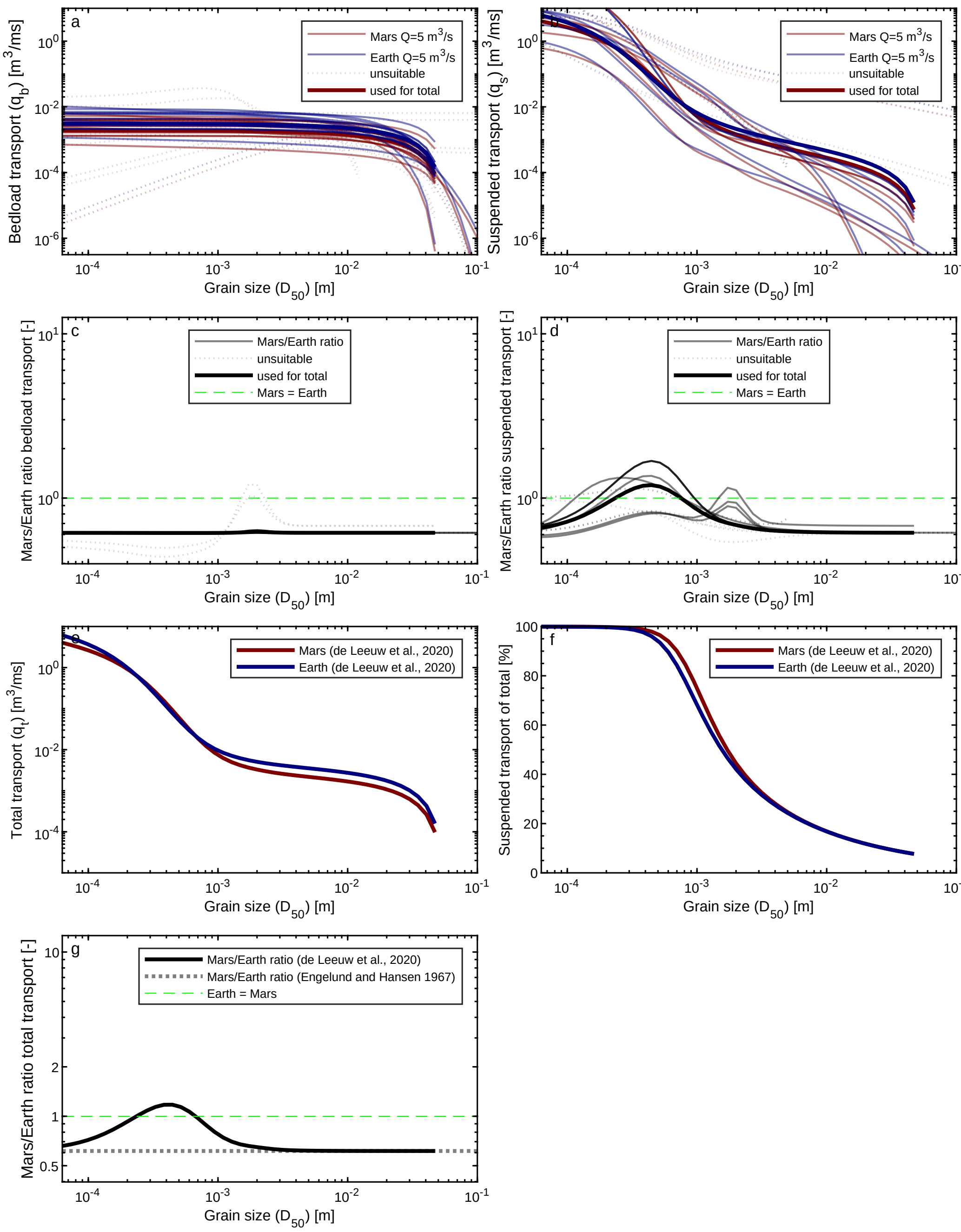

Figure A3. Fluvial transport rates as a function of grain size. (a) Bed load transport q_b $[m^3/ms]$ by formulas indicated in Table 2, (b) suspended transport q_s $[m^3/ms]$ by formulas indicated in Table 2, (c) bed load transport ratio of Mars and Earth $[-]$, (d) suspended transport ratio of Mars and Earth $[-]$, (e) total sediment transport rate q_t $[m^3/ms]$ by total load equations implicitly (Engelund & Hansen, 1967) and explicitly (de Leeuw et al., 2020) including bed load and suspended transport, (f) percentage of suspended transport of the total sediment transport [%], (g) total transport ratio of Mars and Earth $[-]$ for Mars (red) and Earth (blue) gravity acceleration g $[m/s^2]$ and a given water depth h $[m]$ of 5 m and channel geometry.

centuries to millennia. *Earth Surface Dynamics*, *5*(4), 617-652. doi: 10.5194/esurf-5-617-2017

Brown, R. H., Baines, K. H., Bellucci, G., Bibring, J.-P., Buratti, B. J., Capaccioni, F., . . . others (2004). The cassini visual and infrared mapping spectrometer (vims) investigation. *Space Science Reviews*, *115*(1), 111–168. doi: 10.1007/S11214-004-1453-X

Brownlie, W. R. (1981). *Prediction of flow depth and sediment discharge in open channels* (Tech. Rep.). Californa Institute of Technology. doi: 10.7907/Z9KP803R

Burr, D. M., Emery, J. P., Lorenz, R. D., Collins, G. C., & Carling, P. A. (2006). Sediment transport by liquid surficial flow: Application to Titan. *Icarus*, *181*(1), 235–242. doi: 10.1016/j.icarus.2005.11.012

Burr, D. M., Taylor Perron, J., Lamb, M. P., Irwin III, R. P., Collins, G. C., Howard, A. D., . . . others (2013). Fluvial features on titan: Insights from morphology and modeling. *Bulletin*, *125*(3-4), 299–321. doi: 10.1130/B30612.1

Cabrol, N. A., & Grin, E. A. (1999). Distribution, classification, and ages of Martian impact crater lakes. *Icarus*, *142*(1), 160–172. doi: 10.1006/icar.1999.6191

Cabrol, N. A., & Grin, E. A. (2001). The evolution of lacustrine environments on Mars: Is Mars only hydrologically dormant? *Icarus*, *149*(2), 291–328. doi: 10.1006/icar.2000.6530

Cabrol, N. A., & Grin, E. A. (2003). Overview on the formation of paleolakes and ponds on Mars. *Global and Planetary Change*, *35*(3-4), 199–219. doi: 10.1016/S0921-8181(02)00127-3

Camenen, B., & Larson, M. (2005). A general formula for non-cohesive bed load sediment transport. *Estuarine, Coastal and Shelf Science*, *63*(1-2), 249-260. doi: 10.1016/j.ecss.2004.10.019

Cao, Z., Pender, G., & Meng, J. (2006). Explicit formulation of the shields diagram for incipient motion of sediment. *Journal of Hydraulic Engineering*, *132*(10), 1097-1099. doi: 10.1061/(asce)0733-9429(2006)132:10(1097)

Carr, M. H. (2012). The fluvial history of Mars. *Philosophical Transactions of the Royal Society A: Mathematical, Physical and Engineering Sciences*, *370*(1966), 2193-2215. doi: 10.1098/rsta.2011.0500

Carrillo, V., Petrie, J., Timbe, L., Pacheco, E., Astudillo, W., Padilla, C., & Cisneros, F. (2021). Validation of an experimental procedure to determine bedload transport rates in steep channels with coarse sediment. *Water*, *13*(5), 672. doi: 10.3390/w13050672

Celik, I., & Rodi, W. (1984). *A deposition-entrainment model for suspended sediment transport. report no* (Tech. Rep. No. Report No SFB 210/T/6). West-Germany: University of Karlsruhe.

Chatanantavet, P., Whipple, K. X., Adams, M. A., & Lamb, M. P. (2013). Experimental study on coarse grain saltation dynamics in bedrock channels. *Journal of Geophysical Research: Earth Surface*, *118*(2), 1161–1176. doi: 10.1002/jgrf.20053

Cheng, N.-S. (2002). Exponential formula for bedload transport. *Journal of Hydraulic Engineering*, *128*, 942-946. doi: 10.1061/(asce)0733-9429(2002)128:10(942)

Christensen, P. R., Bandfield, J. L., Smith, M. D., Hamilton, V. E., & Clark, R. N. (2000). Identification of a basaltic component on the martian surface from thermal emission spectrometer data. *Journal of Geophysical Research: Planets*, *105*(E4), 9609–9621. doi: 10.1029/1999JE001127

Collins, M. B., & Rigler, J. K. (1982). The use of settling velocity in defining the initiation of motion of heavy mineral grains, under unidirectional flow. *Sedimentology*, *29*(3), 419-426. doi: 10.1111/j.1365-3091.1982.tb01804.x

de Leeuw, J., Lamb, M. P., Parker, G., Moodie, A. J., Haught, D., Venditti, J. G., & Nittrouer, J. A. (2020). Entrainment and suspension of sand and gravel. *Earth*

Surface Dynamics, *8*(2), 485-504. doi: 10.5194/esurf-8-485-2020
De Toffoli, B., Plesa, A. C., Hauber, E., & Breuer, D. (2021). Delta deposits on Mars: A global perspective. *Geophysical Research Letters*, *48*(17), e2021GL094271. doi: 10.1029/2021GL094271
Di Achille, G., & Hynek, B. M. (2010). Ancient ocean on Mars supported by global distribution of deltas and valleys. *Nature Geoscience*, *3*, 459–463. doi: 10.1038/ngeo891
DiBiase, R. A., Limaye, A. B., Scheingross, J. S., Fischer, W. W., & Lamb, M. P. (2013). Deltaic deposits at aeolis dorsa: Sedimentary evidence for a standing body of water on the northern plains of mars. *Journal of Geophysical Research: Planets*, *118*(6), 1285–1302. doi: 10.1002/jgre.20100
Dickson, J. L., Lamb, M. P., Williams, R. M. E., Hayden, A. T., & Fischer, W. W. (2021). The global distribution of depositional rivers on early Mars. *Geology*, *49*(5), 504–509. doi: 10.1130/g48457.1
Edmonds, D. A., & Slingerland, R. L. (2010). Significant effect of sediment cohesion on deltamorphology. *Nature Geoscience*, *3*(2), 105-109. doi: 10.1038/ngeo730
Ehlmann, B. L., Mustard, J. F., Murchie, S. L., Bibring, J.-P., Meunier, A., Fraeman, A. A., & Langevin, Y. (2011). Subsurface water and clay mineral formation during the early history of mars. *Nature*, *479*(7371), 53–60. doi: 10.1038/nature10582
Einstein, H. A. (1942). Formulas for the transportation of bed load. *Transactions of the American Society of civil Engineers*, *107*(1), 561–577. doi: 10.1061/TACEAT.0005468
Einstein, H. A. (1950). *The bed-load function for sediment transportation in open channel flows* (No. 1026). US Department of Agriculture.
Einstein, H. A., Anderson, A. G., & Johnson, J. W. (1940). A distinction between bed-load and suspended load in natural streams. *Eos, Transactions American Geophysical Union*, *21*(2), 628–633. doi: 10.1029/TR021i002p00628
Engelund, F., & Fredsoe, J. (1976). A sediment transport model for straight alluvial channels. *Nordic Hydrology*, *7*(5), 293-306. doi: 10.2166/nh.1976.0019
Engelund, F., & Hansen, E. (1967). *A monograph on sediment transport in alluvial streams* (Tech. Rep.). Copenhagen: Technical University of Denmark.
Fairén, A. G. (2010). A cold and wet mars. *Icarus*, *208*(1), 165–175. doi: 10.1016/j.icarus.2010.01.006
Fassett, C. I., & Head III, J. W. (2008). Valley network-fed, open-basin lakes on Mars: Distribution and implications for Noachian surface and subsurface hydrology. *Icarus*, *198*(1), 37–56. doi: 10.1016/j.icarus.2008.06.016
Ferdowsi, B., Ortiz, C. P., Houssais, M., & Jerolmack, D. J. (2017). River-bed armouring as a granular segregation phenomenon. *Nature communications*, *8*(1), 1–10. doi: 10.1038/s41467-017-01681-3
Ferguson, R. I., & Church, M. (2004). A simple universal equation for grain settling velocity. *Journal of Sedimentary Research*, *74*(6), 933–937. doi: 10.1306/051204740933
Fernandez Luque, R., & van Beek, R. (1976). Erosion and transport of bed-loadsediment. *Journal of Hydraulic Research*, *14*(2), 127-144. doi: 10.1080/00221687609499677
Garcia, M. (1991). Entrainment of bed sediment into suspension. *Journal of Hydraulic Engineering*, *117*(4), 414-435. doi: 10.1061/(ASCE)0733-9429(1991)117:4(414)
Ghail, R. C., Hall, D., Mason, P. J., Herrick, R. R., Carter, L. M., & Williams, E. (2018). Vensar on envision: Taking earth observation radar to venus. *International journal of applied earth observation and geoinformation*, *64*, 365–376. doi: 10.1016/J.JAG.2017.02.008
Golombek, M., Warner, N., Ganti, V., Lamb, M., Parker, T., Fergason, R. L., & Sullivan, R. (2014). Small crater modification on meridiani planum and impli-

cations for erosion rates and climate change on mars. *Journal of Geophysical Research: Planets*, *119*(12), 2522–2547. doi: 10.1002/2014JE004658

Grotzinger, J. P., Gupta, S., Malin, M. C., Rubin, D. M., Schieber, J., Siebach, K., ... Wilson, S. A. (2015). Deposition, exhumation, and paleoclimate of an ancient lake deposit, Gale crater, Mars. *Science*, *350*(6257), aac7575. doi: 10.1126/science.aac7575

Grotzinger, J. P., Hayes, A. G., Lamb, M. P., & McLennan, S. M. (2013). *Sedimentary processes on earth, mars, titan, and venus.* University of Arizona Press. doi: 10.2458/azu_uapress_9780816530595-ch18

Harrison, K. P., & Grimm, R. E. (2008). Multiple flooding events in martian outflow channels. *Journal of Geophysical Research: Planets*, *113*(E02002). doi: 10.1029/2007JE002951

Hauber, E., Platz, T., Reiss, D., Le Deit, L., Kleinhans, M. G., Marra, W. A., ... Carbonneau, P. (2013). Asynchronous formation of Hesperian and Amazonian-aged deltas on Mars and implications for climate. *Journal of Geophysical Research E: Planets*, *118*(7), 1529–1544. doi: 10.1002/jgre.20107

Hayden, A. T., Lamb, M. P., Fischer, W. W., Ewing, R. C., McElroy, B. J., & Williams, R. M. (2019). Formation of sinuous ridges by inversion of river-channel belts in utah, usa, with implications for mars. *Icarus*, *332*, 92-110. doi: 10.1016/j.icarus.2019.04.019

Hayden, A. T., Lamb, M. P., & McElroy, B. J. (2021). Constraining the timespan of fluvial activity from the intermittency of sediment transport on earth and mars. *Geophysical Research Letters*, *48*(16), e2021GL092598. doi: 10.1029/2021GL092598

Hunziker, R. P., & Jaeggi, M. N. R. (2002). Grain sorting processes. *Journal of Hydraulic Engineering*, *128*(12), 1060-1068. doi: 10.1061/ASCE0733-94292002128:121060

Hynek, B. M., Beach, M., & Hoke, M. R. T. (2010). Updated global map of Martian valley networks and implications for climate and hydrologic processes. *Journal of Geophysical Research*, *115*(E9), 1–14. doi: 10.1029/2009je003548

Hynek, B. M., & Phillips, R. J. (2003). New data reveal mature, integrated drainage systems on Mars indicative of past precipitation. *Geology*, *31*(9), 757–760. doi: 10.1130/G19607.1

Itakura, T., & Kishi, T. (1980). Open channel flow with suspended sediments. *Journal of the Hydraulics Division*, *106*(8), 1325–1343. doi: 10.1061/JYCEAJ.0005483

Khawja, S., Ernst, R., Samson, C., Byrne, P., Ghail, R., & MacLellan, L. (2020). Tesserae on venus may preserve evidence of fluvial erosion. *Nature communications*, *11*(1), 1–8. doi: 10.1038/s41467-020-19336-1

Khullar, N. (2007). Transport of fines/wash load through channels–a review. *Hydrology journal*, *30*(3–4), 43–63.

Kleinhans, M. G. (2005). Flow discharge and sediment transport models for estimating a minimum timescale of hydrological activity and channel and delta formation on Mars. *Journal of Geophysical Research: Planets*, *110*(12), 1-23. doi: 10.1029/2005JE002521

Kleinhans, M. G., Leuven, J. R., Braat, L., & Baar, A. (2017). Scour holes and ripples occur below the hydraulic smooth to rough transition of movable beds. *Sedimentology*, *64*(5), 1381-1401. doi: 10.1111/sed.12358

Kleinhans, M. G., van de Kasteele, H. E., & Hauber, E. (2010). Palaeoflow reconstruction from fan delta morphology on Mars. *Earth and Planetary Science Letters*, *294*(3-4), 378–392. doi: 10.1016/j.epsl.2009.11.025

Komar, P. D. (1979). Comparisons of the hydraulics of water flows in Martian outflow channels with flows of similar scale on earth. *Icarus*, *37*(1), 156-181. doi: 10.1016/0019-1035(79)90123-4

Komar, P. D. (1980). Modes of sediment transport in channelized water flows with

ramifications to the erosion of the Martian outflow channels. *Icarus*, *42*, 317–329. doi: 10.1016/0019-1035(80)90097-4
Komar, P. D., & Clemens, K. E. (1986). The relationship between a grain's settling velocity and threshold of motion under unidirectional currents. *Journal of Sedimentary Research*, *56*(2), 258-266. doi: 10.1306/212F88DC-2B24-11D7-8648000102C1865D
Konsoer, K. M., LeRoy, J., Burr, D., Parker, G., Jacobsen, R., & Turmel, D. (2018). Channel slope adjustment in reduced gravity environments and implications for martian channels. *Geology*, *46*(2), 183–186. doi: 10.1130/G39666.1
Kraal, E. R., Asphaug, E., Moore, J. M., Howard, A., & Bredt, A. (2008). Catalogue of large alluvial fans in martian impact craters. *Icarus*, *194*(1), 101–110. doi: 10.1016/j.icarus.2007.09.028
Lamb, M. P., Finnegan, N. J., Scheingross, J. S., & Sklar, L. S. (2015). New insights into the mechanics of fluvial bedrock erosion through flume experiments and theory. *Geomorphology*, *244*, 33–55. doi: 10.1016/j.geomorph.2015.03.003
Lamb, M. P., Grotzinger, J. P., Southard, J. B., & Tosca, N. J. (2012). Were aqueous ripples on mars formed by flowing brines? In *Sedimentary geology of mars* (p. 139-150). SEPM Special Publication No. 102. doi: 10.2110/pec.12.102.0139
Lamb, M. P., McElroy, B., Kopriva, B., Shaw, J., & Mohrig, D. (2010). Linking river-flood dynamics to hyperpycnal-plume deposits: Experiments, theory, and geological implications. *Bulletin*, *122*(9-10), 1389–1400. doi: 10.1130/B30125.1
Lapôtre, M. G. A., & Ielpi, A. (2020). The pace of fluvial meanders on mars and implications for the western delta deposits of jezero crater. *AGU Advances*, *1*(2). doi: 10.1029/2019av000141
Larsen, I. J., & Lamb, M. P. (2016). Progressive incision of the channeled scablands by outburst floods. *Nature*, *538*(7624), 229–232. doi: 10.1038/nature19817
Lee, B. J., Hur, J., & Toorman, E. A. (2017). Seasonal variation in flocculation potential of river water: Roles of the organic matter pool. *Water*, *9*(5), 335. doi: 10.3390/w9050335
Malin, M. C., & Edgett, K. S. (2003). Evidence for persistent flow and aqueous sedimentation on early mars. *Science*, *302*(5652), 1931–1934. doi: 10.1126/science.1090544
Mangold, N., Gupta, S., Gasnault, O., Dromart, G., Tarnas, J. D., Sholes, S. F., ... Williford, K. H. (2021). Perseverance rover reveals an ancient delta-lake system and flood deposits at Jezero crater, Mars. *Science*, *374*(6568), 711-717. doi: 10.1126/science.abl4051
Mantz, P. A. (1977). Incipient transport of fine grains and flakes by fluids—extended Shields diagram. *Journal of the Hydraulics division*, *103*(6), 601–615. doi: 10.1061/JYCEAJ.0004766
McLean, S. R. (1992). On the calculation of suspended load for noncohesive sediments. *Journal of Geophysical Research*, *97*(C4), 5759-5770. doi: 10.1029/91JC02933
Meyer-Peter, E., & Müller, R. (1948). Formulas for bed-load transport. In *Iahsr 2nd meeting, stockholm, appendix 2.*
Meyer-Peter, E., & Müller, R. (1949). A formula for the calculation of bedload transport. *Schweizerische Bauzeitung*, *67*(3).
Miedema, S. A. (2010). Constructing the shields curve, a new theoretical approach and its applications..
Moore, J. M., & Howard, A. D. (2005). Large alluvial fans on Mars. *Journal of Geophysical Research E: Planets*, *110*(4), 1–24. doi: 10.1029/2004JE002352
Murchie, S. L., Mustard, J. F., Ehlmann, B. L., Milliken, R. E., Bishop, J. L., McKeown, N. K., ... others (2009). A synthesis of martian aqueous mineralogy after 1 mars year of observations from the mars reconnaissance orbiter. *Jour-*

nal of Geophysical Research: Planets, *114*(E2). doi: 10.1029/2009JE003342

Nicholas, A. (2013). Morphodynamic diversity of the world's largest rivers. *Geology*, *41*(4), 475-478. doi: 10.1130/G34016.1

Nielsen, P. (1992). *Coastal bottom boundary layers and sediment transport* (Vol. 4). World scientific.

Nixon, C., Lorenz, R., Achterberg, R., Buch, A., Coll, P., Clark, R., ... others (2018). Titan's cold case files-outstanding questions after cassini-huygens. *Planetary and Space Science*, *155*, 50–72. doi: 10.1016/j.pss.2018.02.009

Paphitis, D. (2001). Sediment movement under unidirectional flows: an assessment of empirical threshold curves. *Coastal Engineering*, *43*(3-4), 227-245. doi: 10.1016/S0378-3839(01)00015-1

Parker, G. (1979). Hydraulic geometry of active gravel rivers. *Journal of the Hydraulics Division*, *105*(9), 1185–1201. doi: 10.1061/JYCEAJ.0005275

Parker, G. (1990). Surface-based bedload transport relation for gravel rivers. *Journal of hydraulic research*, *28*(4), 417–436. doi: 10.1080/00221689009499058

Parker, G., Klingeman, P. C., & McLean, D. G. (1982). Bedload and size distribution in paved gravel-bed streams. *Journal of the Hydraulics Division*, *108*(4), 544–571. doi: 10.1061/JYCEAJ.0005854

Peakall, J., Ashworth, P. J., & Best, J. L. (2007). Meander-bend evolution, alluvial architecture, and the role of cohesion in sinuous river channels: A flume study. *Journal of Sedimentary Research*, *77*(3-4), 197-212. doi: 10.2110/jsr.2007.017

Piliouras, A., Lauzon, R., & Rowland, J. C. (2021). Unraveling the combined effects of ice and permafrost on arctic delta morphodynamics. *Journal of Geophysical Research: Earth Surface*, *126*(4). doi: 10.1029/2020JF005706

Porco, C. C., West, R. A., Squyres, S., McEwen, A., Thomas, P., Murray, C. D., ... others (2004). Cassini imaging science: Instrument characteristics and anticipated scientific investigations at saturn. *Space Science Reviews*, *115*(1), 363–497. doi: 10.1007/S11214-004-1456-7

Ribberink, J. S. (1998). Bed-load transport for steady flows and unsteady oscillatory flows. *Coastal Engineering*, *34*(1-2), 59-82. doi: 10.1016/S0378-3839(98)00013-1

Righetti, M., & Lucarelli, C. (2007). May the Shields theory be extended to cohesive and adhesive benthic sediments? *Journal of Geophysical Research: Oceans*, *112*(5). doi: 10.1029/2006JC003669

Rouse, H. (1937). Modern conceptions of the mechanics of fluid turbulence. *Transactions of the American Society of Civil Engineers*, *102*(1), 463–505. doi: 10.1061/TACEAT.0004872

Salese, F., Kleinhans, M. G., Mangold, N., Ansan, V., McMahon, W. J., de Haas, T., & Dromart, G. (2020). Estimated minimum life span of the Jezero fluvial delta (Mars). *Astrobiology*, *20*(8), 977–993. doi: 10.1089/ast.2020.2228

Schmeeckle, M. W. (2014). Numerical simulation of turbulence and sediment transport of medium sand. *Journal of Geophysical Research: Earth Surface*, *119*(6), 1240–1262. doi: 10.1002/2013JF002911

Sharp, R. P. (1973). Mars: Fretted and chaotic terrains. *Journal of Geophysical Research*, *78*(20), 4073-4083. doi: 10.1029/jb078i020p04073

Simões, F. J. (2014). Shear velocity criterion for incipient motion of sediment. *Water Science and Engineering*, *7*(2), 183-193. doi: 10.3882/j.issn.1674-2370.2014.02.006

Smart, G. M. (1984). Sediment transport formula for steep channels. *Journal of Hydraulic Engineering*, *110*, 267-176. doi: 10.1061/(ASCE)0733-9429(1984)110:3(267)

Smith, J. D., & McLean, S. R. (1977). Spatially averaged flow over a wavy surface. *Journal of Geophysical Research*, *82*(12), 1735-1746. doi: 10.1029/JC082i012p01735

Soulsby, R. L. (1997). Dynamics of marine sands: A manual for practical applications. *Oceanographic Literature Review*, *44*(9), 947.

Soulsby, R. L., & Damgaard, J. S. (2005). Bedload sediment transport in coastal waters. *Coastal Engineering*, *52*(8), 673-689. doi: 10.1016/j.coastaleng.2005.04.003

Soulsby, R. L., & Whitehouse, R. J. S. (1997). Threshold of sediment motion in coastal environments. In *Pacific coasts and ports'97. proceedings* (Vol. 1, pp. 149–154).

Vago, J. L., Westall, F., Coates, A. J., Jaumann, R., Korablev, O., Ciarletti, V., ... Carreau, C. (2017). Habitability on early mars and the search for biosignatures with the exomars rover. *Astrobiology*, *17*(6-7), 471-510. doi: 10.1089/ast.2016.1533

van der Vegt, H., Storms, J. E., Walstra, D. J., & Howes, N. C. (2016). Can bed load transport drive varying depositional behaviour in river delta environments? *Sedimentary Geology*, *345*, 19-32. doi: 10.1016/j.sedgeo.2016.08.009

van Ledden, M., van Kesteren, W. G., & Winterwerp, J. C. (2004). A conceptual framework for the erosion behaviour of sand-mud mixtures. *Continental Shelf Research*, *24*(1), 1-11. doi: 10.1016/j.csr.2003.09.002

van Rijn, L. C. (1984a). Sediment transport, part I: Bed load transport. *Journal of Hydraulic Engineering*, *110*(10), 1431-1456. doi: 10.1061/(ASCE)0733-9429(1984)110:10(1431)

van Rijn, L. C. (1984b). Sediment transport, part II: Suspended load transport. *Journal of Hydraulic Engineering*, *110*(11), 1613-1641. doi: 10.1061/(ASCE)0733-9429(1984)110:11(1613)

van Rijn, L. C. (2007). Unified view of sediment transport by currents and waves. i: Initiation of motion, bed roughness, and bed-load transport. *Journal of Hydraulic Engineering*, *133*(6), 649-667. doi: 10.1061/(ASCE)0733-9429(2007)133:6(649)

Wall, S., Hayes, A., Bristow, C., Lorenz, R., Stofan, E., Lunine, J., ... others (2010). Active shoreline of ontario lacus, titan: A morphological study of the lake and its surroundings. *Geophysical Research Letters*, *37*(5). doi: 10.1029/2009GL041821

Wilson, K. C. (1966). Bed-load transport at high shear stress. *Journal of the hydraulics division*, *92*(6), 49–59. doi: 10.1061/JYCEAJ.0001562

Wilson, S. A., Morgan, A. M., Howard, A. D., & Grant, J. A. (2021). The global distribution of craters with alluvial fans and deltas on Mars. *Geophysical Research Letters*, *48*(4), e2020GL091653. doi: 10.1029/2020GL091653

Witek, P. P., & Czechowski, L. (2015). Dynamical modelling of river deltas on titan and earth. *Planetary and Space Science*, *105*, 65–79. doi: 10.1016/j.pss.2014.11.005

Wong, M., & Parker, G. (2006). Reanalysis and correction of bed-load relation of Meyer-Peter and Müller using their own database. *Journal of Hydraulic Engineering*, *132*(11), 1159-1168. doi: 10.1061/ASCE0733-94292006132:111159

Wordsworth, R. D. (2016). The climate of early mars. *Annual Review of Earth and Planetary Sciences*, *44*, 381–408. doi: 10.1146/annurev-earth-060115-012355

Wright, S., Parker, G., & Asce, M. (2004). Flow resistance and suspended load in sand-bed rivers: Simplified stratification model. *Journal of Hydraulic Engineering*, *130*(8), 796-805. doi: 10.1061/(ASCE)0733-9429(2004)130:8(796)

Zanke, U. C. E. (2003). On the influence of turbulence on the initiation of sediment motion. *International Journal of Sediment Research*, *18*(1), 17–31. doi: 10.1016/0029-8018(79)90021-0